Doctoral Dissertation

Studies on Fabrication of Three-Dimensional Micro/Nano Structures in Ionic Liquid Aiming at the Development of New Direct Writing Method

Hiro Minamimoto

January 2015

Department of Applied Chemistry

Graduate School of Engineering

Osaka University

Studies on Fabrication of Three-Dimensional Micro/Nano Structures in Ionic Liquid Aiming at the Development of New Direct Writing Method

（新規直接描画法の開発を目指したイオン液体中での
三次元マイクロ・ナノ構造体作製に関する研究）

2015

Hiro Minamimoto

Department of Applied Chemistry

Graduate School of Engineering

Osaka University

Preface

The studies presented in this thesis were carried out under the guidance of Professor Dr. Susumu Kuwabata at Department of Applied Chemistry, Graduate School of Engineering, Osaka University during 2010-2015.

The purpose of this thesis is to establish a novel new direct writing technology for the field of micro or nanofabrication, which uses liquids as reaction media. Micro/nanofabrication using liquid media is the completely new concept in that region. The author hopes sincerely that the findings obtained in this study would contribute to the progresses of science and technology in the field of both ionic liquid and microfabrication.

Hiro Minamimoto

Department of Applied Chemistry,

Graduate School of Engineering,

Osaka University

Suita, Osaka, Japan

March, 2015

Contents

General Introduction

Recently, direct writing microfabrication methods on semiconductor substrates have been improved greatly and have become important techniques as the micro-electro mechanical system (MEMS).[1–8] The fabrication of fine structures is mainly performed by focused quantum beam irradiation to solid materials under a vacuum condition. The direct writing micro/nano-fabrication methods are categorized into two methods. One is called a top down approach, in which structures are prepared by reforming the surface properties of polymer materials with quantum beam irradiation, and a maximum resolution of around 10 nm can be achieved.[9–14] The other technique is known as a bottom up method, which can build the three dimensional (3D) structures of very complicated shapes that cannot be obtained by the top down method derived from precursors by quantum beam irradiations.[15–19] In both cases, the quantum beam technique is an essential tool for obtaining very fine structures.

The quantum beams, such as an electron beam and an ion beam, is very useful tools because they are easily controlled by either electric or magnetic fields. It is well known that when the beam is irradiated into materials, some kinds of reactive species (i.e., radicals and solvated electrons) are generated in a very small area called “spur”, and these species can easily trigger some chemical reactions.[20–22] In the case of direct writing on polymer surfaces, the bond cleavage or crosslinking reactions occur in the polymer materials, resulting in formation of micro/nano-structures.[23,24] In addition to them, the reactions induced by the reactive species are widely used in various fields,[25–27] and mechanisms for the formation of these species in common solvents have been studied by many radiation chemists.[28–31] Lately, the radiation chemistry of room-temperature ionic liquids (RTILs) has been attracting much attention. RTILs are very interesting materials and have many unique physicochemical properties, for example high conductivity, high thermal stability, a wide electrochemical window, negligible

vapor pressure and so on.[32–36] By using several analytical radiation methods like pulse radiolysis, it has been revealed that the radiolytic yield of solvated electrons in the RTILs was higher than that in typical organic solvents, and RTILs can be used as a good media for the studies of radiolytic reactions such as electron-transfer reactions.[27,37–43]

In more than two decade, RTILs have gained much attention from many researchers in the various scientific and industrial fields because of their unique physicochemical properties.[44–48] Among them, the very low vapor pressure is a quite notable characteristic. Because of the nature of RTILs, they can be introduced into the machines that require vacuum condition such as X-ray photoelectron spectroscopy.[49] Furthermore, as a new analytical method, Kuwabata, Torimoto, and their coworkers have developed a new electron microscope observation technique using RTILs.[50–52] This technology realized the *in-situ* scanning electron microscope (SEM) observations of electrochemical reactions in RTILs, and also succeeded in observing the formation of metal particles generated by electron beam irradiations to RTILs containing metal ions.[53–56] From the latter result, it can be considered that if the radiation reactions could be controlled with nanometer resolution in RTILs by a quantum beam writing system, fabrication of 3D micro/nanostructures could be expected.

The Present Work

The author studied the fabrication of 3D structures in a thin RTIL layer by a focused ion beam (FIB) and electron beam (EB) equipment. The polymer structures fabricated by the irradiation of FIB and EB were obtained and the formation mechanisms for each method were also revealed by ingenuities of irradiation designs and theoretical calculations. In addition to the polymers, the fine metal structures were obtained by EB irradiation to RTIL. All the attempts performed in this study revealed the very unique and innovative points in the structure formation mechanism.

This thesis consists of three chapters as follows:

Chapter 1 deals with the preparation of 3D polymer structures by FIB irradiation. In this process, even intricate three-dimensional micro/nano-structures having overhang and hollow parts can be constructed at the resolution of approximately 100 nm. To reveal the formation mechanism of polymer structures in a polymerizable RTIL by FIB irradiation with raster scanning mode, several approaches like theoretical calculation have been performed.

Chapter 2 introduces a method to fabricate 3D polymer structures by the EB irradiation system. Interestingly, the overall shapes of the obtained structures are different from those prepared by the FIB even if the samples are irradiated in the similar manner. Perceptions obtained in this chapter provide the facile preparation procedures for the micro/nano structures.

In chapter 3, a new silver micro-patterning method by EB irradiation is described. Through this technique, silver deposits are obtained as designed with high resolution and purity compared to the existing direct writing method. The possibility of the method in optical region have also been demonstrated.

Chapter 1

Preparation of 3D Polymer Structures by Focused Ion Beam Irradiation

1-1. Introduction

Focused-ion-beam (FIB) irradiation is a powerful tool for carving the surface of the materials for drawing two-dimensional (2D) patterns by ion sputtering.[57–62] Another fascinating feature is the ability to make up micro- or nanometer size 3D structures by the combination of FIB irradiation and chemical vapor deposition (CVD). This technique known as a FIB-chemical vapor deposition (FIB-CVD) technique needs a reactive gas as a precursor to produce 3D structures. The gas directly introduced into a FIB vacuum chamber is converted into a solid deposit on a substrate by a FIB irradiation.[63] By the approach with a common raster scanning mode, simple standing wire and tube figures can be constructed. However, the fabrication of intricate 3D figures, e.g., overhang and hollow parts, requires a specialized FIB-CVD system, which enables FIB irradiation with a vector mode. Fundamental operating principles of this technique have been developed by S. Matsui and his collaborators.[63–65] The system is designed for providing phenanthrene gas after searching an appropriate voxel, which must be adjacent to a voxel already occupied by a deposit, to produce the 3D figures, because the ion beam irradiation in midair cannot make any contribution to the production as a matter of course. Unfortunately, at this moment, this is not a common technique to fabricate 3D structures.

Liquids such as water and organic solvents are, in general, considered as inappropriate substances for being handled under vacuum condition. Introduction of any type of liquids is,

therefore, strictly prohibited in all instruments, which require vacuum condition, including sputtering equipment, X-ray photoelectron spectroscope, electron microscope, and FIB irradiation instrument. However, the incompatibility between the liquid substances and such instruments is now becoming a thing of the past with the advent of RTILs as described before.

In chapter 1, the new method that can three-dimensionally control the polymerization reaction in a polymerizable 1-allyl-3-ethylimidazolium bis(trifluoromethanesulfonyl)amide ([AllylEtIm][Tf_2N]) RTIL thin layer on a Si wafer was established by using a common FIB technique with a raster scan mode. The formation process of the 3D structures produced by the RTIL-based FIB irradiation method was also examined.

1-2. Experimental section

1-2-1. Preparation of RTILs coated Si-substrate

1-Allyl-3-ethylimidazolium bis(trifluoromethanesulfonyl)amide ([AllylEtIm][Tf_2N]) was purchased from Kanto Chemical Co., Inc. 1-Vinyl-3-butylimidazolium bis(trifluoromethanesulfonyl)amide ([VinylBuIm][Tf_2N]) was synthesized by the previously reported method.[66,67] The chemical structures of each polymerizable RTIL are shown in Fig. 1-1. An n-Si wafer (100 Ω cm^{-2}) purchased from Osaka Titanium Technologies Co., Ltd. was used as a substrate, and the Si surface was modified with (3-aminopropyl)triethoxysilane for improving its affinity to the RTILs.[68] The Si wafer was cut into 1 × 1 cm^2 pieces. The RTILs diluted with ethanol to a concentration of ca. 5 vol% were spread onto the Si wafer to form a very thin and uniform RTIL layer on the Si wafer. After an appropriate amount of the RTIL solution was dropped onto the Si wafer, it was spread by rotation at 4,000 rpm for 5 min. This spin coating technique resulted in a RTIL layer having a thickness of ca. 1 μm, which was confirmed by a confocal laser microscope (VK-8550, Keyence).

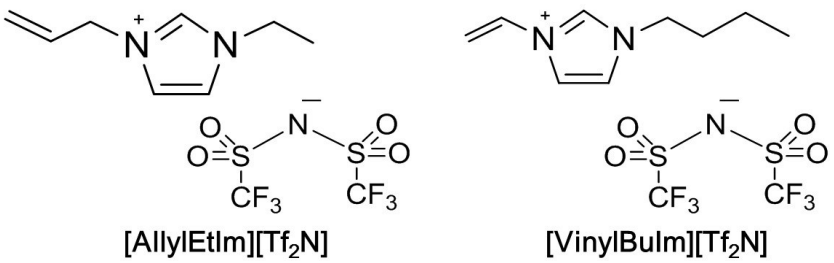

Figure 1-1. Chemical structures of polymerizable RTILs used in this chapter.

1-2-2. FIB Irradiation Experiment

The RTIL-coated Si wafer was introduced into FIB drawing instrument (SMI 2050, Seiko Instruments). A gallium ion beam accelerated at 30 kV was used to irradiate the Si wafer substrate. The ion beam currents and the beam size employed in this chapter were 210 pA and 23 nmΦ, respectively. FIB drawing experiments were conducted by a common FIB irradiation system using a bitmapped image prepared at a display frame of 800 × 800 pixels. The drawing of the images was performed in the raster scanning mode at a 40 μm × 40 μm area. After the FIB irradiation experiment, the Si wafer substrate was repeatedly immersed into acetonitrile bath to remove unreacted RTIL and was dried in air. The obtained structures were observed by a scanning electron microscope (VE-9800, Keyence) operated at an acceleration voltage of 20 kV with electron beam currents between 50 pA and 3.5 nA.

1-3. Results

1-3-1. Polymer Deposits Prepared by RTIL-Based FIB Irradiation Method

The first FIB drawing was characters of "Osaka" onto an [AllylEtIm][Tf_2N] RTIL layer spread on a Si substrate ([AllylEtIm][Tf_2N]/Si). The resulting SEM image of the top view is shown in Fig. 1-2a, indicating that the desired polymer pattern was successfully produced as a result of the local polymerization reaction of the [AllylEtIm][Tf_2N] triggered by the FIB irradiation. Surprisingly, the SEM image from different angles revealed that the characters

are 3D "Osaka" as shown in Fig. 1-2b and that the polymer is formed by a layer-by-layer structure.

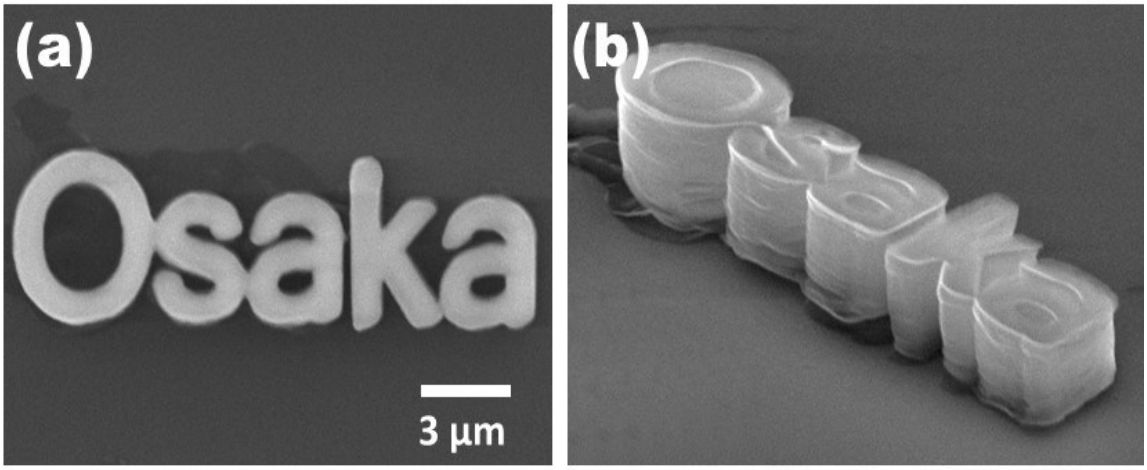

Figure 1-2. SEM images of three-dimensional polymer microstructures. The patterned structures were deposited in a thin [AllylEtIm][Tf_2N] layer on a Si substrate using FIB irradiation with a raster scanning mode. (a) Polymers having "Osaka" characters with a high resolution. (b) Oblique angle image of Fig. 1a shows that these polymer patterns have 3D structures. This polymer patterns were obtained with the ion dose of 300×10^{15} ions cm^{-2} and the number of scanning of 100 times.

To reveal how the polymer grew to the vertical direction, FIB drawings of square frame were performed at different dosages. Figure 1-3a shows a SEM image of the structures obtained on a Si substrate at different doses, D, of 100, 200, 300, 400, and 500×10^{15} ions cm^{-2}. In this investigation, the beam current, I_B, and the dwell time, t_{dw}, were 48 pA and 250 μsec, respectively. The number of pixels, n_{pix}, was 4.0×10^{10} pixels cm^{-2}. The number of raster scan, N, during the FIB drawing experiment is an important parameter for fabricating 3D figures, and the N can be estimated by the following equation:

$$N = \frac{D}{(I_B/e) \times t_{dw} \times n_{pix}} \quad (1)$$

where e is the elementary charge. Therefore, when the D is 100, 200, 300, 400, and 500×10^{15} ions cm^{-2}, the N is 33, 66, 100, 133, and 166 times, respectively. The increase in the N directly

related to the increasing height of the 3D figures, *H*. Figure 1-3b summarizes the relationship between the *H* and the *N* values or the *D* values. The plotted *H* values were calculated by:

$$H = \frac{h}{\sin 75^\circ} \quad (2)$$

where *h* is the value of height obtained from SEM image shown in Fig. 1-2a and 75° is the tilt angle for the SEM observation. The *H* was approximately proportional to the *N* values if it was over 33 cycles; however, no figure was observed by SEM when the *N* was below 33 cycles. The minimum height of the 3D structure was ca. 1.0 μm. As described above, the RTIL was spread onto a Si wafer by a spin coating method so as to obtain a uniform liquid layer with a thickness of ca. 1.0 μm. The maximum height could be expected to depend on the RTIL layer thickness, but it was not. The height continued to increase with the increase in the *N*, and the height apparently exceeded the RTIL layer thickness. For example, at the 166 times, the height became almost 4.3 μm. These results provided a clue to propose the mechanism of 3D pattern formation with this RTIL-based FIB irradiation method, as will be described later.

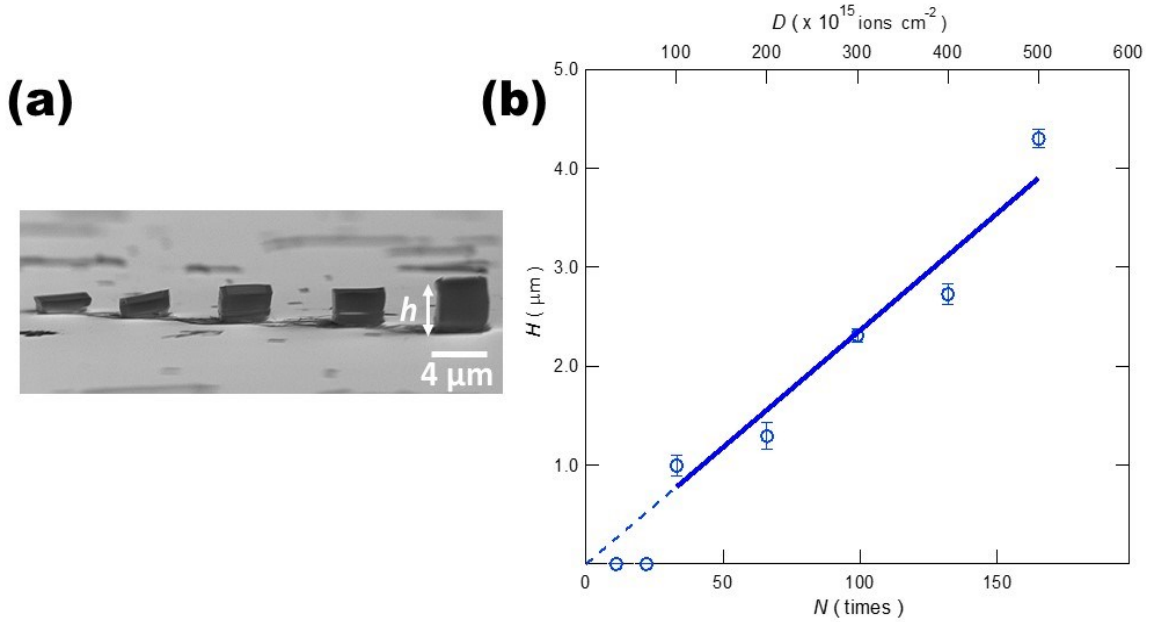

Figure 1-3. Three-dimensional square frame polymer structures prepared under different ion dose conditions. (a) SEM image of square frame structures deposited in a thin [AllylEtIm][Tf_2N] layer on a Si substrate prepared by RTIL-based FIB irradiation method with a raster scanning mode. The image was taken at a tilt angle of 75°. The ion, *D*, doses were 100×10^{15}, 200×10^{15}, 300×10^{15}, 400×10^{15}, and 500×10^{15} ions cm^{-2} from the left to right structure, and then the numbers of scanning estimated from the ion doses, *N*, were 33, 66, 100, 133, and 166 times, respectively. The height of the structures increased with the increase in the *N*, i.e., with the increase in the *D*. (b) Relationship between the heights of the polymer structures and the *N* or the *D*. The polymer structure could not be obtained with the *N* less than 33 times.

1-3-2. Chemical Reactions in [AllylEtIm][Tf_2N] under FIB Irradiation

The deposit obtained by the FIB irradiation onto the [AllylEtIm][Tf_2N] was characterized by a Raman microscope. Raman spectra of the [AllylEtIm][Tf_2N] and the obtained deposit contained some Raman bands in the wavenumber range between 2950 − 3150 cm^{-1} because of the existence of the imidazolium ring (Fig. 1-4a).[69] These results indicate that the imidazolium cations are remained in the deposits produced after the FIB irradiation. In the spectrum of the neat RTIL, the Raman band that is assigned to a stretching vibration of the double bond of the allyl group appeared at 1645 cm^{-1}; however, the band disappeared in the

spectrum of the deposit (Fig. 1-4b). The absence of this band indicates that the polymerization reaction on the allyl group proceeded during the FIB irradiation. In fact, allyl group is known to be difficult to polymerize by a common radical polymerization method, since the allyl radical has a stable resonant structure. Successive radical polymerization reactions are not expected although oligomers are formed.[70] The polymerization reactions observed in this investigation may be peculiar to the [AllylEtIm][Tf_2N] under the FIB irradiation as described below in detail.

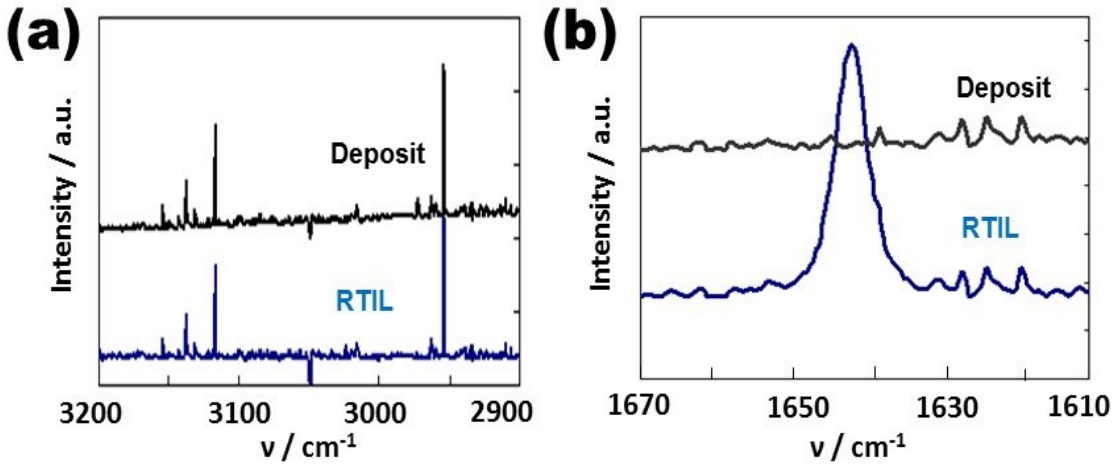

Figure 1-4. Micro-Raman spectra of neat [AllylEtIm][Tf_2N] RTIL and the resulting polymer structure. The wavenumber regions were (a) between 2900 and 3200 cm^{-1} and (b) between 1610 and 1670 cm^{-1}. The spectra obtained at higher wavenumber suggest that imidazolium cation exists in both the neat RTIL and the polymer deposit. The disappearance of the band at 1645 cm^{-1} indicates that the allyl group on the $[AllylEtIm]^+$ is involved in the polymerization reaction.

1-3-3. Resolution of Polymer Deposits

The resolution of the polymer structure produced by the RTIL-based FIB irradiation method was examined through drawing a two-dimensional intricate picture. Figure 1-5a is a photograph of a famous Japanese picture titled "Beauty Looking Back" ("Mikaeri-bijin" in

Japanese) used in this experiment. The original picture was drawn by one of a great Japanese artist, Moronobu Hishikawa, during the Edo period (1603–1868 A.D.) and provided from the Tokyo National Museum. A bitmap file for drawing the FIB irradiation pattern was created by scanning a reproduction of the picture. The bitmap figure is depicted in Fig. 1-5b. As shown in Fig. 1-5c, drawing a microscale "Beauty Looking Back" by using the present approach was achieved. The deposited polymer structure accurately duplicates the bitmap file design. The resolution was approximately 100 nm according to the magnified image of a design on a Kimono, a Japanese traditional dress. This sub-nanometer resolution is one of a great advantage for this RTIL-based FIB irradiation method because other microstructure fabrication methods do not achieve such resolution scale. For example, the resolution of FIB-CVD method is about 200 - 300 nm.[63,71,72]

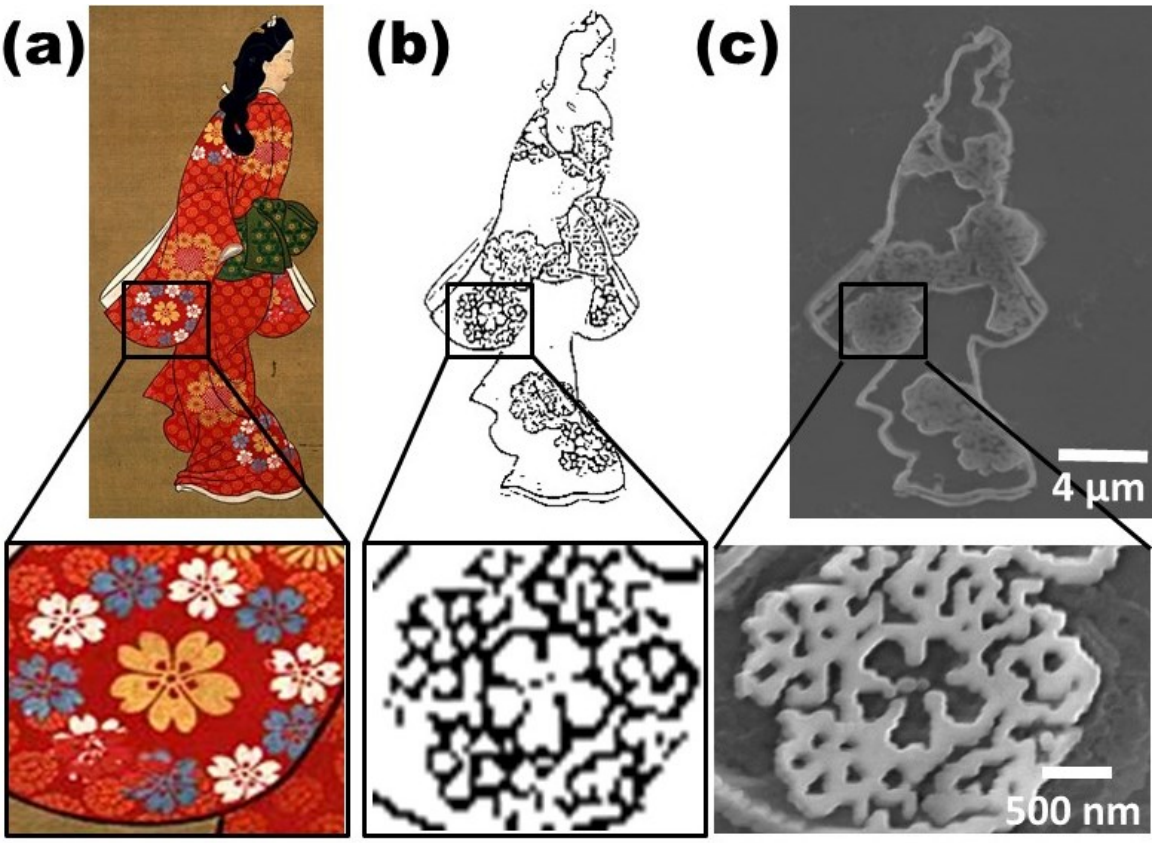

Figure 1-5. Two-dimensional polymer structure prepared by RTIL-based FIB-irradiation method. (a) A famous Japanese picture titled, "Mikaeri-bijin." This picture was painted by a Japanese artist, Moronobu Hishikawa, in the Edo period. (b) Bitmap image of "Mikaeri-bijin" created for the FIB drawing. (c) SEM image of a 2D polymer structure fabricated from the bitmap image. The enlarged view of the flower painted on the "Kimono" is shown under each picture. The irradiation conditions for fabrication of this structure were the ion dose of 100×10^{15} ions cm^{-2} and the number of scanning of 33 times. The patterning “Beauty Looking back” is reprinted with permission from the Tokyo National Museum.

1-3-4. Fabrication of Intricate Three-Dimensional Structures

As mentioned in introduction section, one of the fascinating features of FIB-CVD operated in a vector mode is the ability to produce intricate 3D figures with overhang and hollow parts. The proposed RTIL-based FIB irradiation method that is the combination of the polymerizable RTIL and the common FIB technique with a conventional raster scanning mode can also fabricate complicated 3D figures. These examples are shown in Fig. 1-6. A teacup-shape

was formed by overdrawing different size circles (Fig. 1-6a). A bridge structure, as shown in Fig. 6b, was constructed by drawing two separate square frame patterns, followed by drawing another square frame pattern so as to bridge the previously prepared 3D patterns. Even like a jack-in-a-box structure shown in Fig. 1-6c could be fabricated. It was composed of five 3D square frame patterns; firstly one 3D square pattern was deposited as a base, and after that four slightly smaller 3D square frame patterns were separately drawn by the FIB in order to position one side of each smaller square on one of the four sides on the top of the base square. The structure with long hanging structures, which are technically impossible to prepare by a FIB sputtering method, was eventually prepared. The four overlapped structures were equally formed at four sides on the top of the base square, indicating that the formation of the hanging structure occurs irrespective of the direction of the raster scanning. Formation of a photonic crystal-like 3D network structure (woodpile structure) was also succeeded by the same approach (Fig. 1-6d).

Another complex structure was designed to find a clue about the formation mechanism of the 3D structures by the RTIL-based FIB irradiation method. This structure was prepared by deposition of a rectangular frame base, followed by drawing of two square frame patterns; one square frame was located adjacent to the base, and another was put its one side on one side of top of the base rectangle structure (Fig. 1-7a). Apparently the former pattern was directly deposited onto the Si wafer (Fig. 1-7b), whereas the latter was formed onto the base structure (Fig. 1-7c). The formation of the hanging structure suggests that the polymerization reaction occurs at the position higher than the previously prepared deposit because the latter frame pattern did not deposit on the Si substrate although the FIB drawing was initiated from left bottom as shown in Fig. 1-6a.

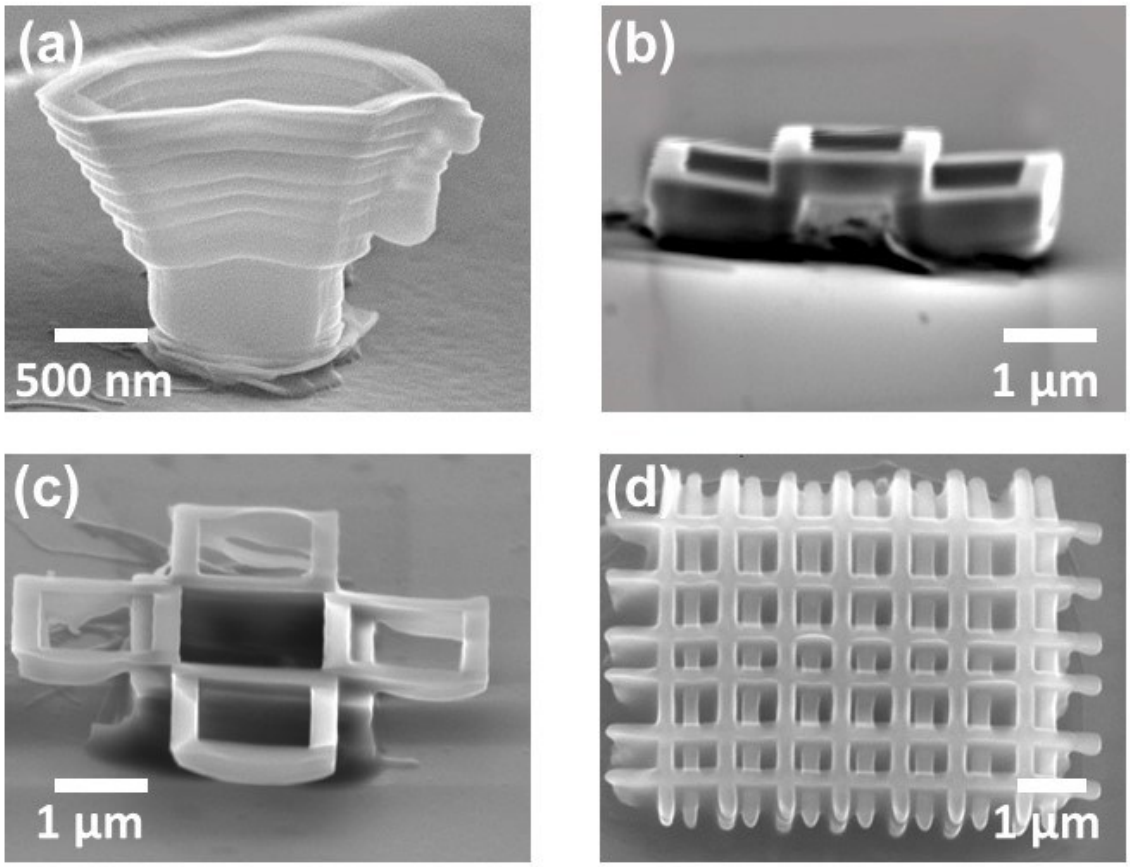

Figure 1-6. Various three-dimensional polymer structures. (a) Teacup structure. The structure was achieved by stacking circle patterns in layers. (b) Bridge structure. The structure has a hollow construction. The two square frame structures were prepared first, and another square frame structure was drawn at the center so as to overlap the previously deposited two square figures. (c) A jack-in-a-box structure. The four upper square frame structures protrude from the base one. This result shows that overhang structures were formed without depending on the scanning directions. (d) Woodpile structure. This structure is known as one of the 3D photonic crystals. These structures were obtained by RTIL-based FIB irradiation method with a raster scanning mode.

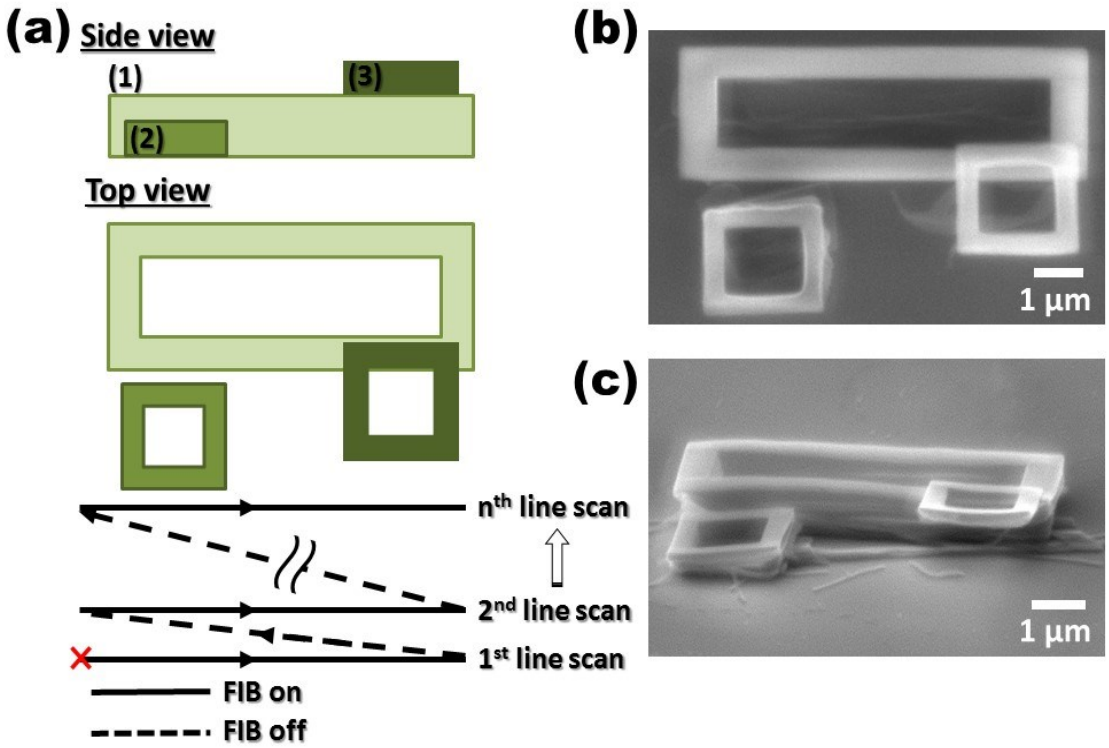

Figure 1-7. Complicated three-dimensional polymer structures. (a) Drawing design for fabrication of the polymer patterns shown in Fig. 1-6b and c. First, the large rectangular frame structure (1) was drawn as a base. Second, the small square frame structure (2), which did not overlap the base polymer, was drawn at the left side of the base. Finally, another small square frame structure (3) was prepared on the base, but only one side of the small square overlapped on part of the base. The FIB irradiation with a raster scanning was initiated from the **X**. The direction was indicated by the arrows. (b) SEM image of polymer structures prepared by the design depicted in Fig. 1-6a. (c) Oblique angle image of Fig. 1-6b. This SEM image indicates the small square frame structure on the right side protrudes from the base, although another small square on the left side is on the substrate.

1-4. Discussion

As is well known, ion beam irradiation to polymer materials including polyethylene and polystyrene generates radicals that come from hydrocarbon backbones, and then cross-linkage reaction among the backbones proceeds.[73–76] It is highly likely that similar cross-linkage reaction occurs among the $[AllylEtIm]^+$ oligomers yielded during the FIB irradiation. As a

result, rigid polymer derived from the [AllylEtIm][Tf_2N] would be obtained. In order to investigate other non-volatile polymerizable RTIL for the RTIL-based FIB irradiation method, the same experiment was performed by using 1-vinyl-3-butylimidazolium bis (trifluoromethanesulfonyl)amide ([VinylBuIm][Tf_2N]) that has an easily polymerizable vinyl group. Because polymerization rate for linear polymers without crosslinks of vinyl groups is much faster than the oligomerization of allyl groups, it was very difficult to control the polymerization reaction induced by the FIB irradiation. It is then likely that the reaction proceeded three-dimensionally beyond the irradiated position. The resulting polymer structures on the [VinylBuIm][Tf_2N]/Si are shown in Fig. 1-8. Both SEM and optical microscopic observation revealed that many irregular structures exist around the FIB-irradiated positions. From these results, we concluded that [AllylEtIm][Tf_2N] is much better than [VinylBuIm][Tf_2N] when 3D polymer structures are constructed by this approach that is called RTIL-based FIB irradiation method. Therefore, it can be said that the RTIL with the allyl group is the most suitable for the RTIL-based FIB irradiation method at this time.

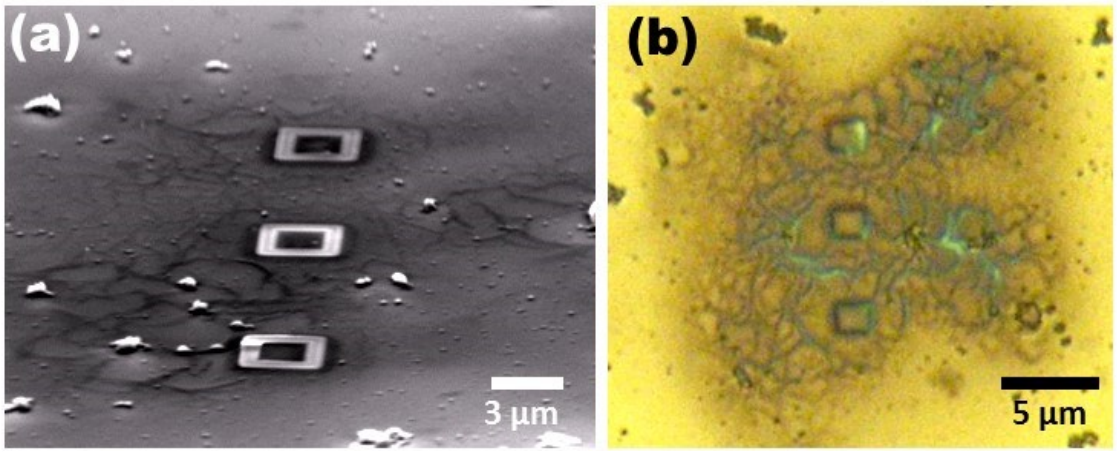

Figure 1-8. Polymer structures deposited with the RTIL-based FIB irradiation method using [VinylBuIm][Tf_2N]. (a) Oblique angle SEM image of square frame patterns. These deposits were very thin, and unexpected irregular deposits existed around the FIB-irradiated positions. It is highly possible that the deposits are formed by high polymerization reactivity of vinyl groups. (b) Optical microscope image of the same sample. This polymer patterns were obtained with the ion dose of 100 × 10^{15} ions cm^{-2} and the number of scanning of 33 times.

As described above, some 3D structures were produced over the RTIL film thickness (ca. 1 µm). It can be explained by the surface tension of the RTIL itself. Figure 1-8 indicates SEM images of the prepared square frame patterns before and after rinsing the unreacted [AllylEtIm][Tf_2N] off using acetonitrile. All the prepared patterns were designed to be about 2.0 µm high. Before rinsing, the deposited patterns were completely covered with the RTIL, due to the surface tension of the RTIL (Fig. 1-9a and 1-9b). But after removing RTILs, the square frame patterns exceeding the original RTIL layer thickness of ca. 1.0 µm appeared (Fig. 1-9c).

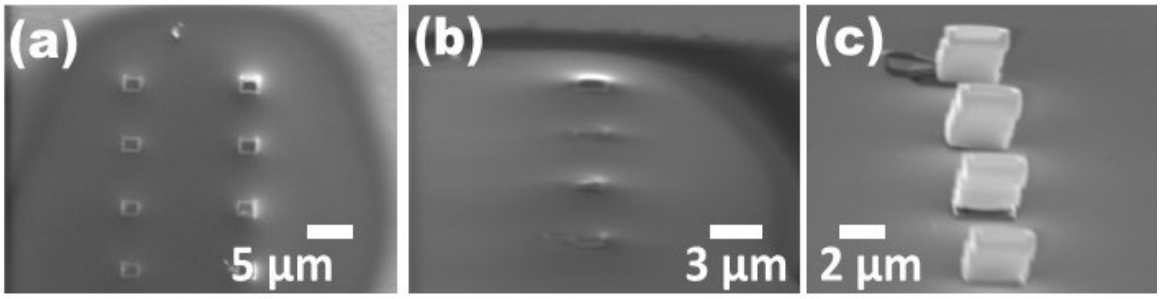

Figure 1-9. SEM images of three-dimensional square frame structures covered with and without RTIL. (a) SEM image of several square structures before rinsing off the [AllylEtIm][Tf_2N] RTIL. (b) Another SEM image taken from a different angle. The meniscus derived from the surface tension was observed on the polymer patterns. All the structures were covered with the RTIL layer. (c) SEM image of Fig. 1-8b after rinsing the RTIL off using acetonitrile. The height of the structures exceeded the RTIL layer thickness of ca. 1 μm. The irradiation conditions for fabrication of this structure were the ion dose of 300×10^{15} ions cm^{-2} and the number of scanning of 100 times.

On the basis of several findings in this chapter, a plausible formation process for 3D polymer structures by the RTIL-based FIB irradiation method was proposed. As depicted in Fig. 1-9, at the initial stage, polymerization reaction of the [AllylEtIm][Tf_2N] proceeds by FIB irradiation at the surface of the RTIL layer, and polymer layer is formed in accordance with the design programmed in advance (Fig. 1-10). When the FIB drawings are repeated, the polymer deposit grows downward until it reaches the Si wafer (Fig. 1-10b and 1-10c). If the bottom of the polymer structure reaches the Si wafer, it physically adheres to the Si wafer. It is also possible that some chemical bondings via Si-OH contribute the adhesion. Once the structure is immobilized onto the Si wafer, subsequent FIB irradiation causes a further polymerization on the immobilized structure (Fig. 1-10d-f). Because RTIL exists on the top of the polymer structure owing to the meniscus derived from the surface tension of the RTIL as described in the preceding paragraph, the height does not depend on the RTIL layer thickness. In some cases those were over 4 μm high. Therefore the RTIL-based FIB method make it possible to

fabricate a wide variety of 3D micro- or nanostructures with hanging and bridging parts but not produce the polymer structure that is less than ca. 1 μm high as shown in Fig. 1-3 because the structure is not immobilized until it reaches the Si wafer. Monte Carlo simulation on the gallium-ion travel distance through the RTIL strongly supports the idea that the polymerization reaction occurs at the surface of RTIL.[77] For understanding the formation mechanism of the three-dimensional structure, we theoretically calculated the gallium-ion range in [AllylEtIm][Tf_2N]. The ion range is a linear distance from the surface of the target to the position where incident ions loss their kinetic energy. In the classical method, the ion range (R) can be estimated from the stopping power, (*dE/dx*), and the *dE/dx* is calculated using Bethe–Bloch formula1. The formulas for calculating these factors are;

$$R = \int_0^{E_0} \frac{1}{dE/dx} dE \quad (3)$$

$$-\frac{dE}{dx} = \frac{4\pi Z_1^2 e^4}{m_0 v_1^3} N_{ad} Z_2 \ln\left[\frac{2m_0 v_1^2}{I(1-\beta^2)} - \beta^2\right] \quad (4)$$

where Z_1 and Z_2 are the atomic number of incident ion and effective atomic numbers of target specimen, respectively, e is the electronic charge, m_0 is the electron mass, v_1 is the velocity of the charged particle, β is v_1/c (c: light speed), N_{ad} is the atomic density of the target, and I is the average ionization energy. However, this calculation does not consider the scattering behavior caused by collisions between incident ions and atoms in the target specimen. Therefore, to estimate the ion range more precisely, Monte Carlo simulation method, which takes account of the scattering angle, is widely employed for such calculation now. Stopping and Range of Ions in Matter (SRIM) is the most famous and powerful computer program series for calculating ion ranges by Monte Carlo simulation method.[77] Detailed information on the calculation is available elsewhere.[77,78] Several parameters, such as ion type, ion energy and

target density, must be inputted before running the program. In the present case, the target density, i.e., the density of [AllylEtIm][Tf_2N], was 1.46 g cm^{-3} at 298 K. The gallium-ion range in the [AllylEtIm][Tf_2N] calculated by SRIM 2013 was approximately 40 nm, which is substantially smaller than the thickness of ca. 1 μm; that is, the polymerization reaction theoretically proceed only at the vicinity of the RTIL surface.

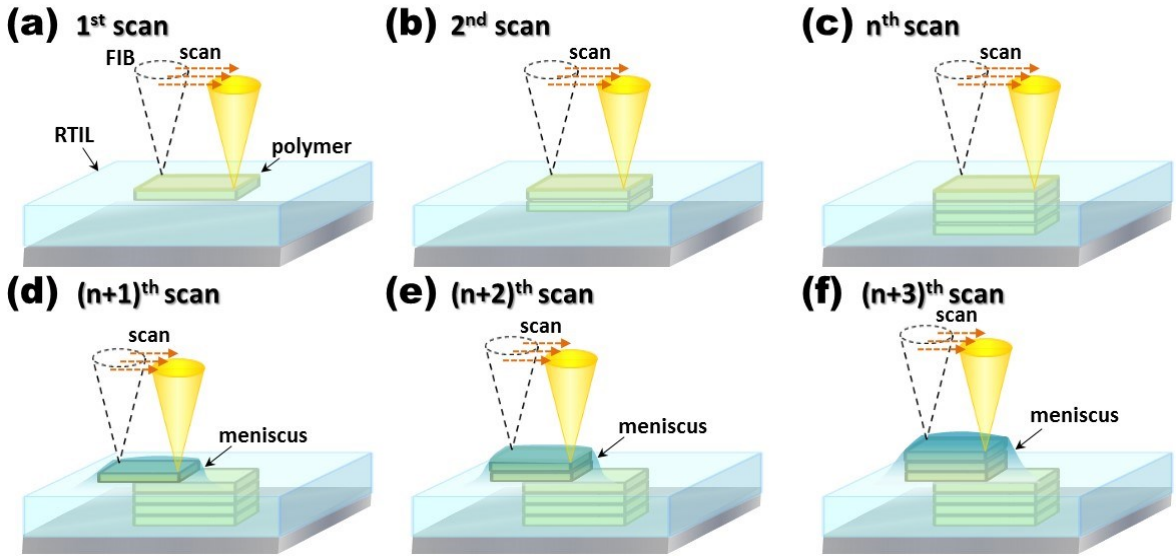

Figure 1-10. Schematic illustrations of a plausible three-dimensional polymer structure formation process by RTIL-based FIB irradiation method. (a) At the initial stage, polymerization reaction proceeds by FIB irradiation at the surface of the polymerizable RTIL, [AllylEtIm][Tf_2N], and a polymer layer is formed. (b) The deposit grows downward until it reaches the Si substrate, when the FIB drawings are repeated. (c) After the deposit reached the Si wafer, it physically adheres to the substrate. (d - f) Once the structure is immobilized onto the Si wafer, subsequent FIB irradiation causes further polymerization on the immobilized structure due to the surface tension with meniscus of the RTIL. Finally, a three-dimensional polymer structure is produced by RTIL-based FIB irradiation method with a raster scanning mode.

1-5. Conclusions

In conclusion, the combination of the polymerizable [AllylEtIm][Tf_2N] and the FIB

irradiation with a raster scanning mode enabled the preparation of micro/nanoscale 3D polymer structures. The interesting feature is that another polymer structure can be deposited on the top of the premade polymer deposit with ease as the 3D printers, which are rapidly becoming popular in several fields. Even the intricate polymer structure with hanging and bridging parts was produced at the resolution of approximately 100 nm. Thus, the RTIL-based FIB irradiation method reported in this article will make a large contribution to further development of the MEMS/NEMS technology and make the 3D polymer micro/nanostructure fabrication closer to many scientists and engineers.

Chapter 2

Fabrication of 3D Polymer Structures by Electron Beam Irradiation

1-1. Introduction

The electron beam (EB) irradiation technique is considered as a very important technique because of its high resolution on the order of less than 5 nm. Nowadays, the electron beam lithography process has been a key technology for fabricating nanoelectromechanical systems and has achieved under 10 nm.[79–84] The EB has an advantage over the FIB in terms of higher resolution, although its energy density is lower. So far, many resist materials have been developed such as chemical amplified resists.[14,85–88] In the investigations, however, the concept of "using liquids for fabrication of micro structures" has never been proposed because of their vapor pressure.

The aim of this chapter is, in order to extend the previous FIB method described in previous chapter and to propose the present technique as a new direct writing method, to employ an EB writing system for the micro/nano fabrication of polymer structures from an allyl-type polymerizable RTIL ([AllylEtIm][Tf_2N]). As a result, various 3D micro/nano polymer structures having high aspect ratio up to 5 with a resolution of sub-100 nm were able to be prepared and the structures obtained by this method have higher resolution compared to the FIB method. To the best of my knowledge, this is the first achievement that can control the polymerization of monomers in sub-100 nm scale.

2-2. Experimental section

2-2-1. Preparation of the RTIL-coated Si Wafer

The sample preparation method was almost the same as the procedure described in chapter 1. [AllylEtIm][Tf_2N] was also used in this chapter. Silicon atoms existing at a surface of the Si wafer which was purchased from Osaka Titanium Technologies Co., Ltd. were terminated with hydroxyl groups by a UV/ozone treatment. To improve the affinity to the RTILs, Si wafer was modified with 3-aminopropyltriethoxysilane (APTES). APTES aqueous solution (1 vol%) was placed on the substrate for 10 min,[89] followed by rinsing with ultrapure water. The appropriate amount of the RTILs diluted with ethanol (5 vol%) was dropped on the substrate and spun at 4000 rpm for 5 min. The thickness of the obtained liquid film was estimated by the reflectance measurement to be approximately 1 μm.

2-2-2. EB Irradiation Experiment

The EB patterning was performed by a scanning electron microscope (JEOL-9100, JEOL Ltd.) equipped with a pattern generator (SPG-924, Sanyu Electron Co., Ltd.). EB irradiation was carried out in a vacuum chamber with its pressure kept under 9.6×10^{-5} Pa. The acceleration voltage was 30 kV, and the beam current was adjusted from 1,000 to 5,000 pA. The shapes of drawing patterns were prepared in bitmap format (5000 × 5000 pixels) and fit into the irradiation area of 50 μm square. Accordingly, the scale for one pixel becomes 10 nm square. The EB was irradiated following the bitmap image in the raster scanning mode, and the scan rate was adjusted to give a designated electron dose. No recognizable changes of the pressure in the vacuum chamber were observed during the irradiation. After the EB exposure, the substrate was rinsed with acetonitrile to remove the unreacted RTIL, and then dried in air. The prepared polymer patterns were observed by the SEM with an acceleration voltage between 5 and 20 kV without metal coating. An infrared spectrum was recorded by an FT-IR spectrometer (FT/IR-6200, JASCO) and that for the microstructure was measured

with an optional IR microscopy equipment (IRT-7200, JASCO). Raman spectra for both an ionic liquid and a deposited polymer were measured by a Raman microscope (RAMAN-11, Nanophoton).

2-2-3. Measurement of Young's Modulus

The force curve measurements were performed with a scanning probe microscope (NanoNaviReal, SII nanotechnology). A silicon cantilever (SI-DF20P) with a typical force constant of 9 N/m was employed. Prior to the force curve measurements, topographic images were recorded by the tapping mode. Five arbitrary points were chosen for each polymer structure and the repulsive forces were recorded as a function of *Z* motion of sample stage. The force curves were fitted with the equation[90] by using an in-house procedure running on Igor Pro 6.3 (Wavemetrics Inc.) and the Young's modulus were estimated.

2-3. Results

2-3-1. Fabrication of 3D Structures by EB Irradiation onto the Allyl-type RTIL

The fabrications of 3D polymer structures from [AllylEtIm][Tf_2N], which was the same as the RTIL used in combination with FIB irradiation, were first demonstrated in the form of drawing some images and characters. Figure 1-1 shows SEM images of the deposited polymers resulted from irradiation of EB onto the [AllylEtIm][Tf_2N] layer that was spun on the APTES-modified Si wafer. The fine structures were obtained according to the irradiation pattern with a uniform thickness as large as 800 nm. Additionally, the magnified image also shows that this method achieves the resolution as small as around 200 nm. As judged from the rigid nature of the structures that were retained on the substrate even after multiple rinsing, some chemical bonds may be formed between the polymer and surface modifier during the irradiation more than a simple physisorption. The irradiated dose per unit area was 30

mC/cm^2 (900 J/cm^2), which is much higher than that used for EB lithography with commercially available resist like ca. 10 μC/cm^2 (300 mJ/cm^2) in the case of negative type SU-8.[11] Besides the intrinsic reason that the polymerization of monomers needs higher electron dose than cross-linking reactions, the need for such the large amounts of dose is due to the low reactivity of allyl group leading to cross-linking chain transfer as well known. Incidentally, we could not obtain any structures when the irradiation dose was less than 20 mC/cm^2; there was a definite threshold to obtain a solid deposition probably due to the requirement of generating the insoluble oligomers and low-molecular-weight polymers.

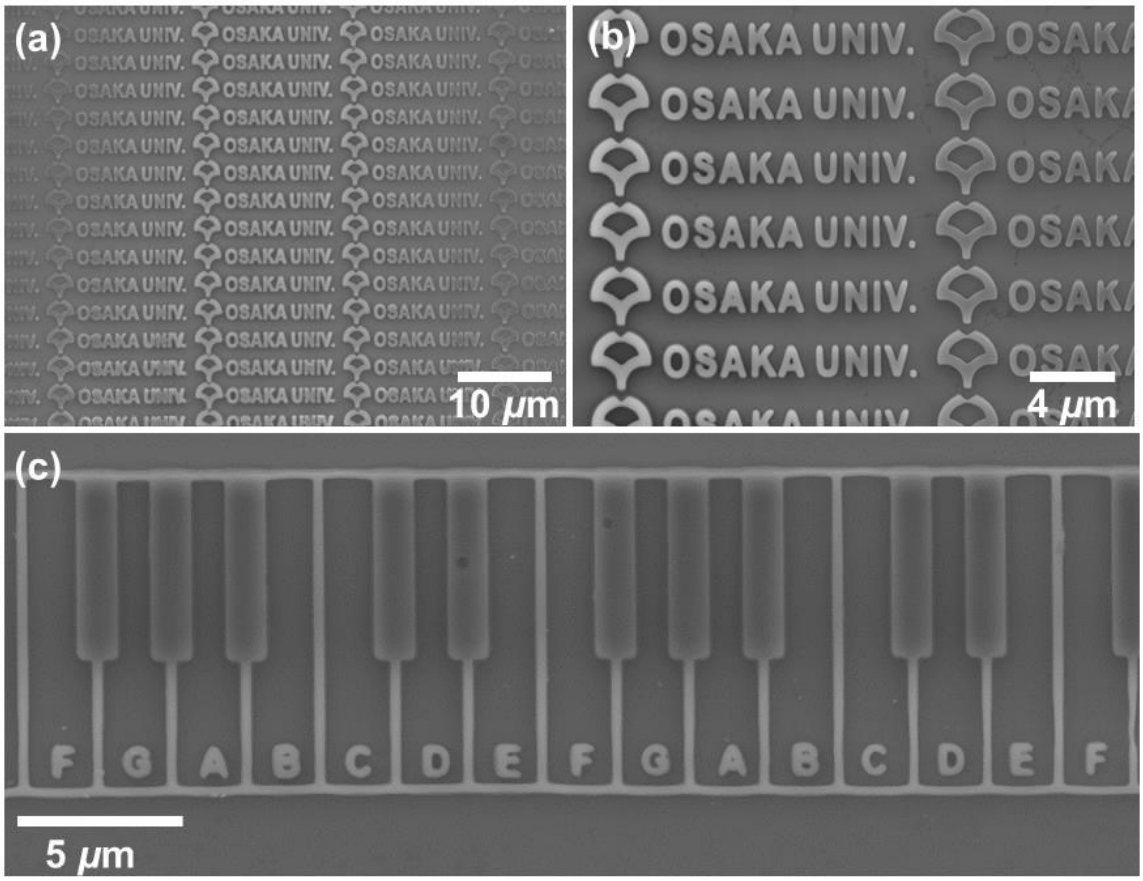

Figure 2-1. SEM images of polymer structures prepared by EB irradiation to [AllylEtIm][Tf_2N]; (a) "OSAKA UNIV." characters prepared in the area of 50 μm square, (b) the magnified image of (a), (c) keyboard layout. All the structures were prepared with 30 mC/cm^2 dose condition.

Polymer line structures as illustrated in Fig. 2-2 were fabricated to demonstrate the resolution of the resulting polymer pattern. Eleven lines with different line width were aligned parallel to each other with two thick vertical lines that were formed prior to the formation of the horizontal lines in order to maintain the uniformity of the RTIL thickness of this area. SEM images for the thus formed polymer structures were shown in Fig. 2-2 with the dose per unit area given to make each structures. The first thing we should mention is that not all the lines were formed as irradiated. In the cases of 250 and 200 mC/cm^2, the two narrowest horizontal lines (10 and 20 nm) were not obtained, and when the dose was reduced to 150 mC/cm^2, the line of 30 nm width was also absent. As mentioned in the experimental section, the line of 10 nm width corresponds to that of one pixel width; in other words, the electron beam is scanned one time in the raster scanning mode used in a series of experiments. These results indicate that not only the dose per unit area but also the consecutive irradiation of EB to adjacent positions have some influence on the formation of solid structures, which is quite unexpected if the nature of liquids and the typical scan interval (about 0.3 sec) were considered. It is also noteworthy that difference in the width between the irradiation pattern and the obtained polymer pattern for the horizontal lines became large with an increase in dose, while those for vertical lines became small.

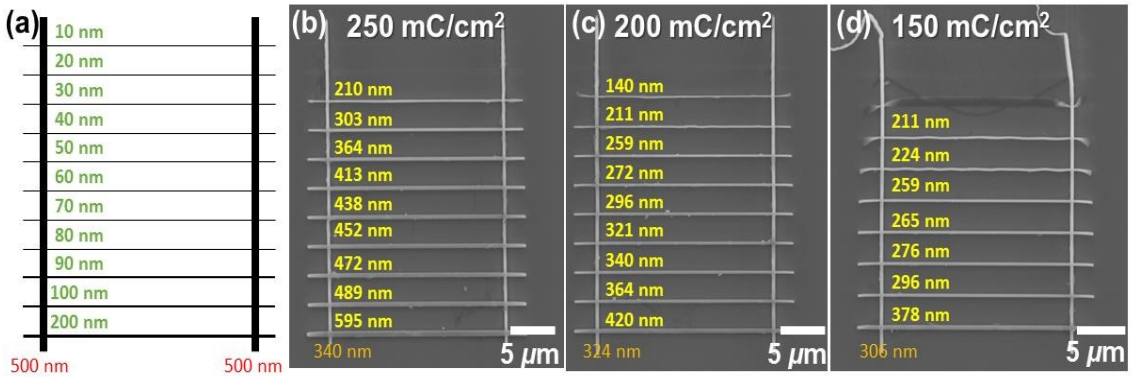

Figure 2-2. Line patterns prepared to check the resolution; (a) irradiation design with the numbers indicating the width of each line: red for horizontal lines and green for vertical lines. (b–d) SEM images of deposited structures prepared with the dose conditions of (b) 250, (c) 200, and (d) 150 mC/cm^2. The numbers in orange and green indicate the actual line widths of the obtained structures for horizontal and vertical lines, respectively.

SEM images in Fig. 2-3 show cross-shaped patterns comprised of horizontal and vertical lines. The irradiation design of each line has 60 nm and 80 nm width, respectively. It must be noted that the horizontal lines were first drawn, followed by drawing the vertical lines; the irradiation dose for the both lines were 200 mC/cm^2, which is large enough to obtain polymers from the perspective given above. SEM images from different angles were also shown in Fig. 2-3c and 2-3d. Even the both structures were fabricated with the same condition; there was a distinct difference in height between them. The dose may not be an exclusive factor that decides the thickness of the structure.

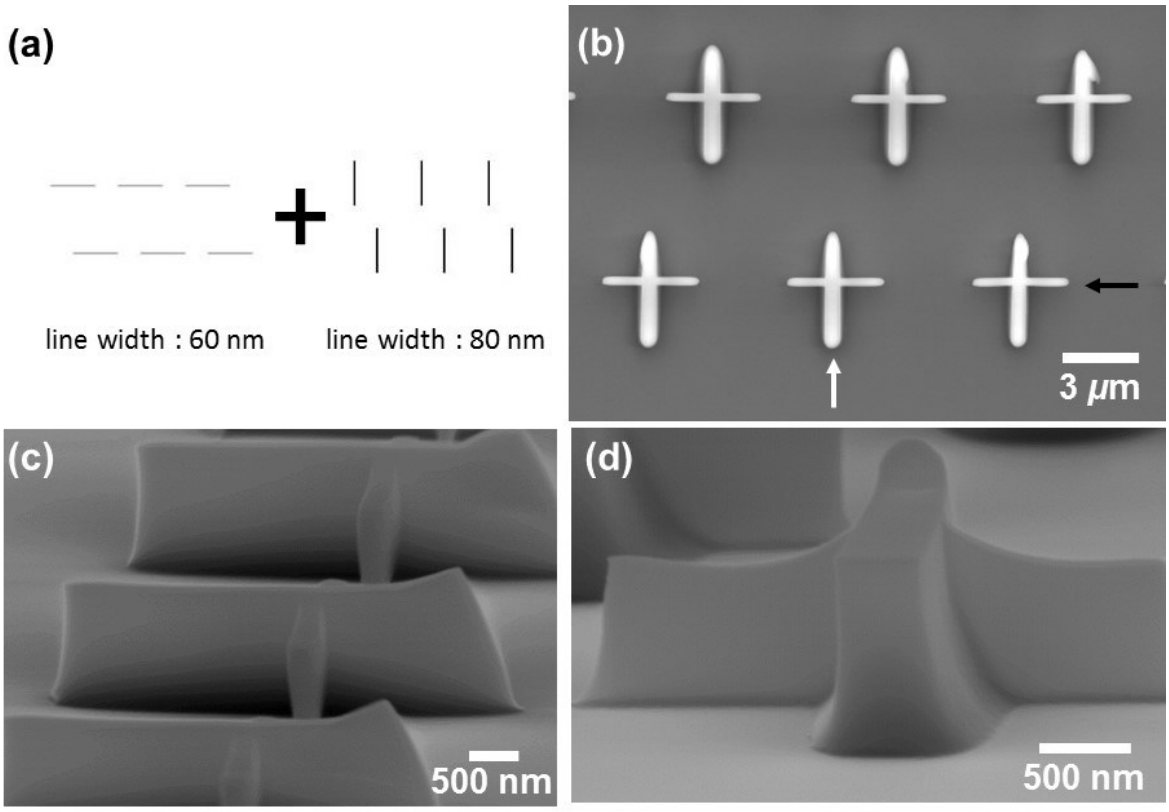

Figure 2-3. Cross shaped structures prepared by two-step irradiation; (a) irradiation design indicating the two-step irradiation, (b) top-view SEM image of deposited structures, (c, d) side-view SEM images observed from the direction represented in (b) by (c) black and (d) white arrows. Dose condition was 200 mC/cm^2.

In order to investigate the effect of two-step irradiation on the deposited shape and to compare the present method to previous FIB method, EB was irradiated by following the irradiation design that we have used in the previous FIB experiment. The structures in Fig. 2-4 were comprised of five square frames; a bigger center frame was first prepared, followed by four smaller frames with one side of each frame being overlapped with the center frame. Unlike the jack-in-a-box-like structures prepared by the FIB irradiation with raster scanning (see Fig. 1-6c in chapter 1), all the frames were attached on the Si substrate independent of the order of irradiation, as if they have grown from the substrate. It is one of the most important differences that were seen between FIB and EB irradiations.

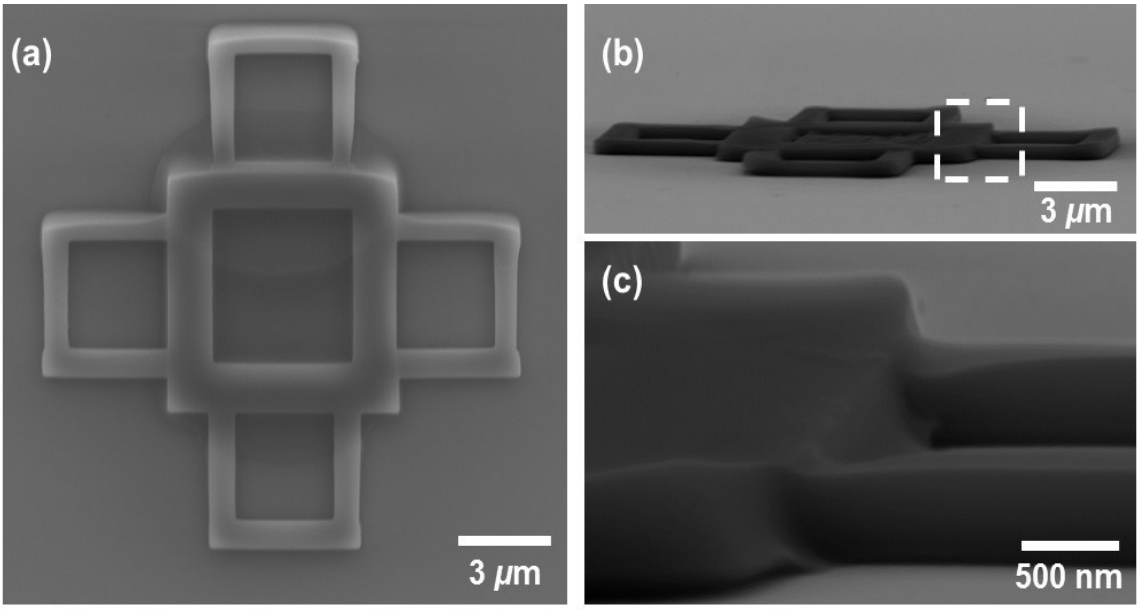

Figure 2-4. SEM image of frame structure comprised of five squares; (a) top view, (b) side view, and (c) magnified image of the square in (b). Dose condition was 30 mC/cm^2.

2-3-2. Characterization of the Deposited Polymer Structures by FT-IR Spectroscopy

To understand the chemical reactions, the structures in Fig. 2-1 were characterized by FT-IR microscopic analysis. The beam size of the IR microscope was confined to ten micrometers square by an aperture and a part of the structure was measured. The IR spectra for both the [AllylEtIm][Tf_2N] monomer and deposited structures were shown in Fig. 2-5a and 2-5b. In the spectrum of the monomer, the multiple peaks around 3100 cm^{-1} derive from C–H stretching of the imidazolium cation. The absorption band around 1136 cm^{-1} was assigned to the C–N symmetric and asymmetric stretching of the imidazolium side chain, and the sharp peak at 1624 cm^{-1} and multiple peaks around 1452 cm^{-1} derive from the ring vibration of imidazolium. The C=C stretching for allyl group arise as a small peak at 1649 cm^{-1}. On the other hand, vibrations for [Tf_2N] anion are observed at 3636, 3552, 1356, 1190, and 1056 cm^{-1}. After the

EB irradiation to [AllylEtIm][Tf_2N], the IR spectrum changed drastically. The most distinctive difference is the broad absorption between 2500 cm^{-1} and 3500 cm^{-1} that is attributable to the N−H stretching of amines (including some coupled, overtone vibrations) in complicated chemical environment.[91] The small peak arising from allyl group disappeared, while absorptions corresponding to [Tf_2N] were almost unchanged. The disappearance of the allyl group was also confirmed by the micro Raman spectra that was more sensitive to the C=C double bond (Fig. 2-5c). These results indicate that the majority of radiation-induced reaction occurs on the cation, leading to the cleavage of C–N bonds for side chains[92] and to oligomerazation of allyl group. Cross-linking reaction may also occur to form the deposits during continuous irradiations of EB with relatively high dose.

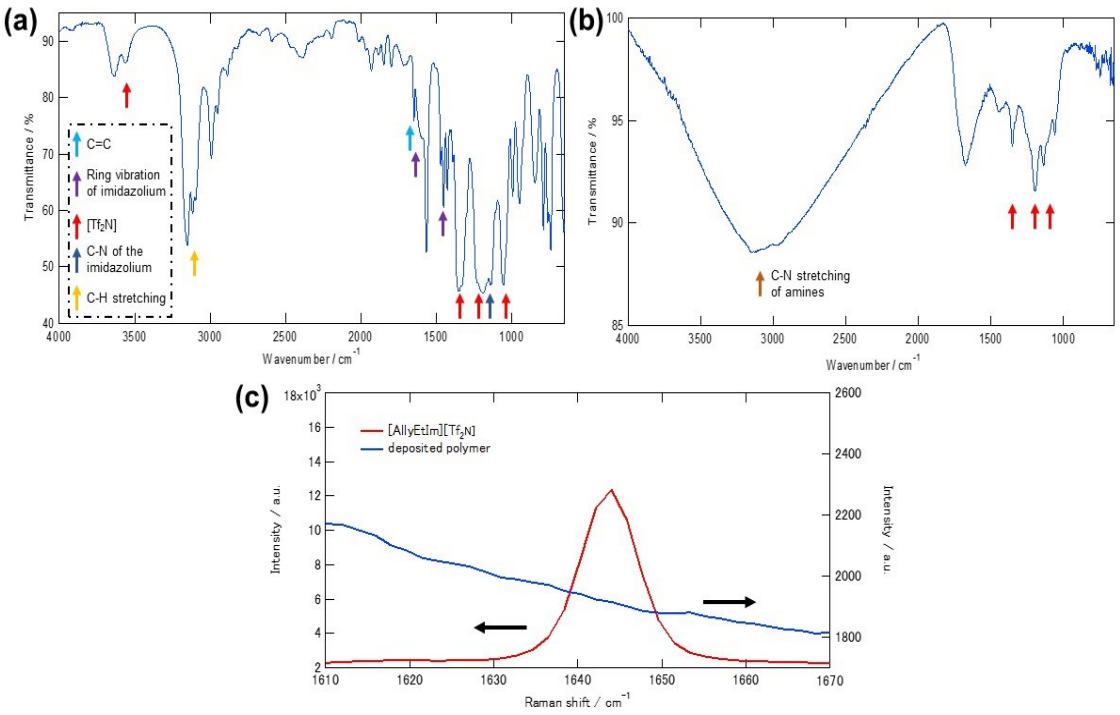

Figure 2-5. (a) FT-IR spectrum of [AllylEtIm][Tf_2N], (b) FT-IR microscopic measurement for the deposited polymer structures and (c) the micro Raman spectra of deposited polymer structures (Ex. 532 nm). The red and blue lines indicate the RTIL monomer and deposited polymer, respectively.

2-3-3. Measurement of Young's Modulus by AFM

The elastic properties of the deposited polymer were examined by AFM in the force curve mode, which measures the repulsive force from the sample indented by a cantilever. The displacement of the cantilever, $z - z_0$, and sample distortion, $d - d_0$, can be associated with the following equation;[90]

$$z - z_0 = d - d_0 + \sqrt{\frac{k(d - d_0)}{\left(\frac{2}{\pi}\right)[E(1 - v^2)]\tan(\alpha)}} \qquad (1)$$

where k is the spring constant of the cantilever, E is the Young's modulus of the sample, α is the half-opening angle of the cone (= 16°), and v is a Poisson ratio that is equal to 0.5. The cantilever's spring constant k was estimated by the equation 1 based on the force curve on a Si-substrate having a known elasticity of E = 185 GPa. Then, the Young's modulus of the samples were estimated by fitting the force curves to the equation. More detailed information about this method has been reported by Radmacher.[90]

The elasticity of the structures made with six different irradiation conditions are listed in Table 1; five points were chosen at random for each structure. No discernible difference could be identified from SEM observations between these points of measurement. At first glance, the deposited polymers had the nonuniform structures with different Young's modulus by location. However, the elasticity of each polymer was still correlated with the dose amount and beam current when they are compared as an average. Commercially available polymers, such as polyethylene and polyethylene terephthalate, have the Young's modulus around 10 GPa.[93] In all current conditions between 1 to 5 nA, the amounts of dose seemed to have a major effect on the elasticity of the samples. The structures prepared with 100 mC/cm^2 were much harder than those deposited with 50 mC/cm^2. It can be easily expected that the chemical structures of the polymer may be changed by long time EB irradiations. It is also notable that the number of relatively hard points, for example, E > 50 GPa for 50 mC/cm^2 and E > 100 GPa

for 100 mC/cm^2, became large with the increase in the beam current, suggesting that not only dose but also beam current have effects on the physical properties of polymer.

Table 2-1. The results of Young's modulus measurements for each polymer structures

Measuring points	Polymer structures deposited by beam current of 1 nA		Polymer structures deposited by beam current of 2.5 nA		Polymer structures deposited by beam current of 5 nA	
	E (Gpa) for 50 mC/cm^2	*E* (Gpa) for 100 mC/cm^2	*E* (Gpa) for 50 mC/cm^2	*E* (Gpa) for 100 mC/cm^2	*E* (Gpa) for 50 mC/cm^2	*E* (Gpa) for 100 mC/cm^2
1	6.0	80	0.2	12	2.3	70
2	1.4	40	50	180	0.3	100
3	0.5	80	25	50	15	3.5
4	<0.1[(a)]	1.0	<0.1[(a)]	150	30	100
5	<0.1[(a)]	40	180	30	40	60

(a)Fitting reliability is low for soft samples less than 0.1 GPa

2-4. Discussion

It is commonly known that the allyl groups are hardly polymerized because generated radicals are too stable to keep successive radical polymerization reactions.[70] However, solid structures were obtained by the FIB irradiation to the allyl-functionalized RTIL, which was reported recently with a possible mechanism of the chemical reactions. [AllylEtIm][Tf_2N] oligomers were considered to be first formed by the repeated ion beam irradiation, followed by the cross-linking reaction between these oligomers. Thus, the rigid polymer structures have

been obtained from the allyl-functionalized ionic liquid. The same reactions may also be induced by the irradiation of EB. The results of FT-IR and Young's modulus measurement, which revealed that giving larger dose lead to the formation of stiff structures with complicated chemical structure, show the occurrence of cross-linking reaction and support the prognosis.

One of the important points for the present technique is that it is possible to make any shapes of deposits precisely by a single raster writing of images. Even if the total area exceeds 50 μm square, the obtained structure had a resolution of several tens of nanometers. The resolution of polymers produced by EB irradiation was further examined by using the image shown in Fig. 2-2a. The most notable thing is the absence of some lines. In the case of 250 and 200 mC/cm^2, for example, at least three scans were required to obtain the polymer structure, indicating the cumulative effect of three adjacent temporally-spaced shots. This in itself is not such strange if it was considered that the spatial spread of electron range around several tens of nanometers in radius, as will be mentioned later, increases the net dose of the overlapped place. In such the case, however, the active species must stay at the same position and alive during the scanning interval of typically 0.3 sec. Calculation from the diffusion coefficient of RTILs, which is on the order of 1×10^{-11} m^2 s^{-1}, predicts that the reactive species generated in spurs can travel ca. 1 μm from the irradiated positions during that interval time.[94] In addition, the lifetime of reactive species that is about several tens of microseconds is too short to maintain its chemical reactivity over the repetitive scans.[95] Therefore, it is the most plausible that the oligomers having much lower diffusivity than monomers are formed during the first and second scan, and then they are deposited to form the rigid structure by the third scan.

Unignorable differences between irradiation line width and actual width of the corresponding deposits should be considered. It is quite reasonable to consider the traveling of electrons after they hit the material. The electron range, which means the distance from

the surface of the target to the position where irradiated electrons completely lose their energy, can be calculated by the following equation;

$$R = 2.1 \times 10^{-12} \times \frac{E_0^2}{\rho} \qquad (2)$$

where E_0 (eV) is the energy of irradiated electrons and ρ (g/cm^{-3}) is the density of the target. In the case of [AllylEtIm][Tf_2N] with the density of ρ = 1.46 g/cm^{-3}, the electron range is estimated to be approximately 13 μm, which is much larger than the RTIL layer thickness as small as 1 μm. Of course, a lateral displacement should also occur by the electron scattering during the traveling within the RTIL layer. The Monte Carlo simulation was, therefore, employed to draw trajectories of multiple sets of electrons by supposing two layer model consisting of 1 μm RTIL and a Si-wafer (density; 2.3 g/cm^{-3}) as a bottom layer.[96] As shown in Fig. 2-6a, a large part of electrons penetrate the RTIL layer and reach the Si substrate with the expansion of beam diameter in RTILs due to the elastic and inelastic scatterings. The lateral spreading of electrons reaches up to several tens of nanometers, and it becomes obvious at high dose amount. These perceptions coincided with the results shown in Fig. 2, where high dose amount gave thick structures even if the same irradiation pattern was used. In other words, a high resolution structure can be obtained by the appropriate choice of the dose amount. In fact, the structures made for demonstration (Fig. 1) was prepared with much lower dose (30 mC/cm^2) than that displayed in Fig. 2-2 and 2-3 comprised of narrower lines. Together with the perceptions mentioned above, preparation of the bulky structure needs less dose because the oligomers have many chances to be solidified by the EB irradiated in close proximity.

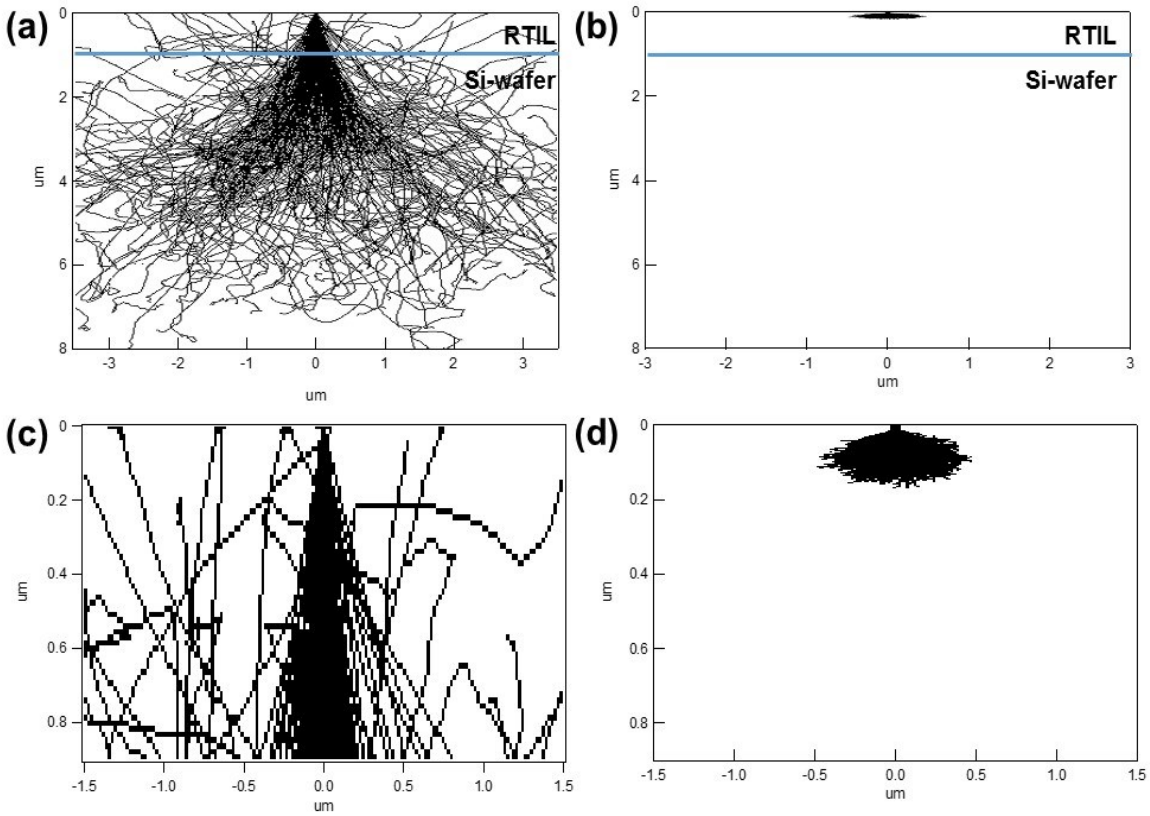

Figure 2-6. The Monte Carlo simulation for (a) the electron range and (b) the ion range. The images of (c) and (d) are the magnified graphs for the RIIL layer of (a) and (b), respectively. The number of incident electrons and ions were 10,000. The displayed electron number is 200. The thickness of an RTIL layer was 1 μm and the density of [AllyEtIm][Tf_2N] was 1.46 g cm^{-3}. The black lines were the trajectory of incident particles. These simulations were performed by CASINO and SRIM 2008, respectively.

The polymer structures shown in Fig. 2-3 provide another interesting point of view. The tilt SEM images show that the line structures have a high aspect ratio up to around 5. Such a high-aspect ratio can only be obtained by recently developed new resist materials such as an epoxy chemistry-based EB resists and chemically amplified resists.[14,85,86] The easiness of the rinsing process that is intrinsic to the liquid matrix may contribute to the achievement because, in the conventional lithographic processes, mechanical stress between the developed structures and non-reacted polymer matrix often damage the spindly part of structures during the rinse process.[97] This stressless situation seemed to bring another advantage that is the

smoothness of the sidewalls, roughness of which was hardly recognized in the SEM images shown in Fig. 2-3. The difference in height between the horizontal and vertical lines should also be discussed. Although the dose amount was the same for the both cases, the vertical lines were higher than the horizontal ones. This may derive from the alteration of the RTIL thickness that was pushed up by the pre-deposited horizontal structures, making the second vertical structures grow higher than the horizontal ones. Such the phenomenon seems to be unique to the liquid phase reaction and could not be observed for the case of the common resist materials. Furthermore, the horizontal structures were gently curving at around the intersection with the vertical lines, as shown in Fig. 2-3d, probably because the growth around the curving area was initiated from the top of the existing horizontal line during the preparation of the vertical lines. This can be predicted from the result of the Monte Carlo simulation. These behaviors are very different from not only the conventional lithography but also from previous FIB-RTIL method, in which the two step exposure can realize complicated 3D structures including a hollow and a reverse taper structures.

The structure shown in Fig. 1-4 is a typical example that expresses the differences between the EB and FIB methods. Although, in the FIB method, the four smaller squares were deposited on the center square so as to be completely lifted from the Si substrate (see Fig. 1-5c), all of the five frames were deposited on the substrate when the EB was used. For understanding of these different phenomena, the Monte Carlo simulation was also performed for the diffusion of Ga ion beam at 30 kV in the RTIL layer and was displayed in Fig. 2-6(b).[77] In the case of ion beam irradiations at accelerating voltage of 30 kV, the Ga ion range was considerably smaller than the electron range because of its strong interaction with atoms in the target RTIL. Therefore, as shown in Fig. 2-7, it can be concluded that the polymers prepared by the FIB irradiation form at the interface of vacuum and RTIL, while in the case of the EB irradiation, the large part of electrons penetrate the RTIL layer and the polymerization and

cross-linking reaction occur at whole irradiated area of the RTIL at once. By considering all results which were obtained in the present chapter, the difference between EB-RTIL and FIB-RTIL method, and also found the utility of each quantum beam RTIL methods was clarified.

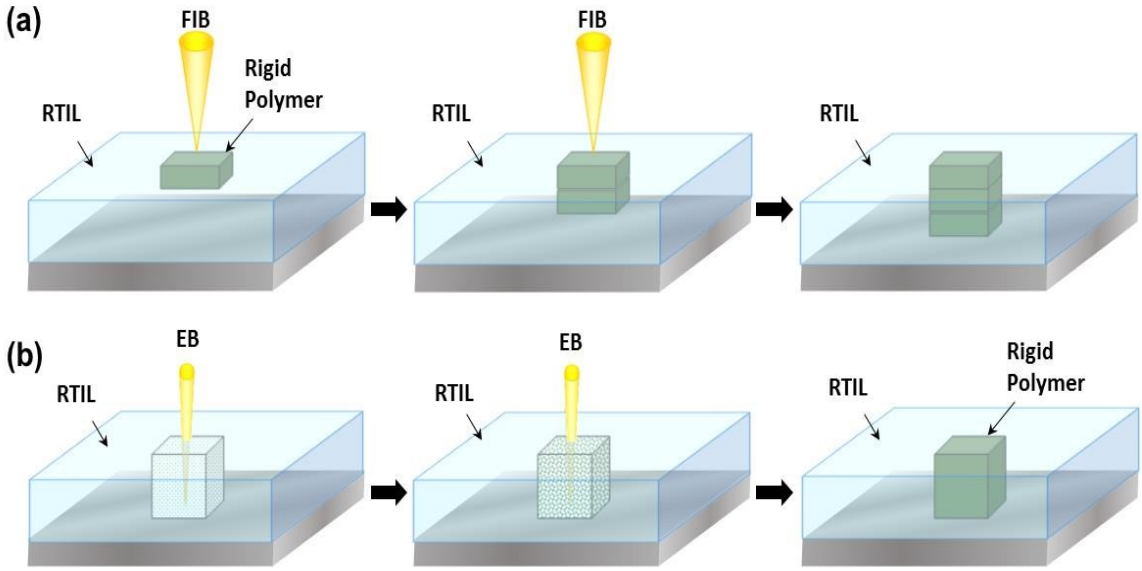

Figure 2-7. Illustrations of the polymer formation mechanism for (a) FIB-RTIL method and (b) EB-RTIL method. In the case of FIB method, the polymer structures deposited at the surface of RTIL. On the contrary, the polymer patterns were formed between the substrate and RTIL by EB irradiation.

2-5. Conclusion

The fine polymer structures with high aspect-ratio and high resolution over the area as large as 50 μm square were obtained by introducing the allyl-type polymerizable RTIL into the EB drawing system. In addition, the effect of irradiation dose and beam current on the physicochemical properties of the deposited polymers was investigated by measuring the FT-IR spectra and Young's modulus. Interestingly, the overall shapes of the obtained structures were different from those prepared in previous chapter using a focused ion beam (FIB) even if

the samples were irradiated in a similar manner. This may be due to the different transmission between the two types of beams as discussed on the basis of the theoretical calculations of the quantum beam trajectories. Perceptions obtained in this chapter provide the facile preparation procedures for the micro/nano structures. From all results given in this chapter, the idea of a completely new direct-writing technique have been proposed and this development would become a viable technology for the fabrication of micromachines or microelectronic devices.

Chapter 3

Preparation of Silver Structures by Electron Beam Irradiation

3-1. Introduction

Fabrication of micro/nano metal structures on semiconductor substrates is an essential technique for the development of the MEMS.[98–100] To date, there have been many achievements for the patterning of metals, such as gold, silver and copper.[101–106] Among them, the direct writing techniques are considered as the most efficient method because of their simplicity of the process. They include direct drawing by the inkjet printing,[107–110] or reactive deposition from precursors contained in liquids[111–114] and those existing in the gas phase by using lasers and a quantum beam[17,115–119], respectively. The last case using the quantum beam achieved resolution as small as 100 nm. However, liquids are considered to be advantageous because they can provide larger amount of metals in a short time compared with the vapor phase deposition.

Recently, the group which the author belongs has reported the preparation of various kinds of colloidal metal nanoparticles dispersed in RTILs by γ-ray radiation irradiation.[44,120] By this method, getting metal dispersed RTILs became quite easy. The similar reduction reactions were observed during the electron microscopic observations (20–300 kV), where the metal nanoparticles were formed on the surface of or inside the ionic liquids around the observation area. These investigations gave the new idea of metal direct writing technology to the author.

In the previous chapters, the fabrication of various three dimensional micro/nano polymer

structures was demonstrated by introducing the thin layer of polymerizable RTIL into a quantum beam writing system to trigger the polymerization reaction of RTIL monomers at nano scale. In this chapter, a new direct writing technique that deposits metals at will on a substrate by introducing RTILs containing silver salts was proposed instead of polymerizable ones. The largest difference is the role of RTIL, which was a reactant previously, as a reaction media for silver deposition. Therefore, how to provide an appropriate amount of silver ions, and how to fix a metallic silver on a substrate that was floating on the RTIL with an uncontrolled irradiation, can be issues to be solved. Micro-scale silver patterns are very promising in terms of their catalytic activity[121] and a potential to the plasmonic applications like the surface-enhanced Raman scattering (SERS).[122] The approach described in this chapter affords to make fine silver patterns of high resolution and purity within a shorter period of time than the deposition from the gas phase. Also, compared with template-based methods, possibility to obtain an arbitrary shape will be beneficial to the plasmonic researches and applications.

3-2. Experimental section

3-2-1. Chemicals

The RTIL, *N*,*N*,*N*-trimethly-*N*-propylammonium bis(trifluoromethanesulfonyl)amide ($[N_{1,1,1,3}][Tf_2N]$), was purchased from Kanto Chemical Co., Inc. It was washed with water and chloroform, then dried under vacuum condition at 100 °C for 24 h prior to use. $H[Tf_2N]$ (Morita Chemical Industries Co., Ltd.), Ag_2O (>98%, Kishida Chemical Co., Ltd.), 3-aminopropyltriethoxysilane (>98%, Sigma-Aldrich Co. LLC), and rhodamine 6G (>99%, Sigma-Aldrich Co. LLC) were used without further purifications. The $Ag[Tf_2N]$ was synthesized by mixing $H[Tf_2N]$ and Ag_2O following the previously reported method.[123] An n-Si wafer (100 Ω cm^{-2}) purchased from Osaka Titanium Technologies Co., Ltd. was used as a substrate. Water used in the present chapter was purified with Milli-Q Integral 3 (18.2 MΩ

cm).

3-2-2. Preparation of RTIL-Coated Si Wafer

The sample preparation procedure was almost the same as described in previous chapters. The Si substrate was cleaned in SC1 solution (NH_3aq : 30% H_2O_2 : H_2O = 1 : 1 : 4) at 60 °C for 20 min, followed by the termination with hydroxyl groups by UV/ozone treatment. For improving the affinity of the substrate to both the RTIL and deposited Ag patterns, Si wafer was modified with 3-aminopropyltriethoxysilane (APTES). For this purpose, the substrate was immersed in an anhydrous toluene solution containing 1 vol% APTES for 12 h, followed by rinsing with an ultrapure water. Ag[Tf_2N] was dissolved in [$N_{1,1,1,3}$][Tf_2N] in 390 mM, and diluted with ethanol to be 5 vol%. An appropriate amount of the solution was dropped on the substrate and spun at 4000 rpm for 5 min. The thickness of the obtained liquid film was approximately 1 μm.

3-2-3. EB Irradiation Experiment

The EB irradiation was performed by a scanning electron microscope (SEM, JEOL-9100, JEOL Ltd.) equipped with a pattern generator (SPG-924, Sanyu Electron Co., Ltd.). The acceleration voltage and beam current was set to 30 kV and 2500 nA, respectively. The vacuum condition was kept under 9.6×10^{-5} Pa during the whole irradiation processes. Bitmap images consisting of 5000 × 5000 pixels were prepared and loaded on the pattern generator. The EB was irradiated following the image with the raster scanning mode in the area of 50 × 50 μm.

3-2-4. Characterizations of Deposited Structures

After the EB irradiation, the RTIL was removed by rinsing with acetone. The deposited

structures were observed by an SEM (Keyence, VE-9800) equipped with energy dispersive X-ray analysis (EDAX Genesis-XM2, EDAX). EDX line analyses for the Ag line patterns was also performed as shown in Fig. 3-2. The Raman spectra were recorded by a Raman microscope (RAMAN-11, Nanophoton) before and after the post-treatment with 1 M HNO_3 aqueous solution.

3-3. Results and Discussion

3-3-1. Fabrication of Silver Structures and Discussion about the Structure Formation Mechanism

Figure 3-1 shows Ag patterns deposited on a 3-aminopropyl trimethoxysilane (APTES) modified Si substrate by irradiating 30 kV focused EB onto the RTIL thin layer of 1 μm thickness. The EB was raster scanned from left to right toward the bottom direction of the images with the irradiating dose of 1200 J/cm^2. The substrate was modified with APTES to improve the affinity of both the RTILs and Ag patterns for the Si substrate.[124] The RTIL used in the experiment was *N*,*N*,*N*-trimethyl-*N*-propylammonium bis(trifluoro-methanesulfonyl)amide ($[N_{1,1,1,3}][Tf_2N]$) containing silver bis(trifluoro-methanesulfonyl)amide ($Ag[Tf_2N]$) in 390 mM, although details for experimental conditions are provided in the experimental section. The SEM images were obtained after removing RTILs by acetonitrile. Firstly, making line structures by the EB swept along the lines, i.e., from left to right in the image of Fig. 3-1a, was attempted. Judging from the SEM images, Ag structures consisted of very small particles. These Ag structures stuck to the substrate strongly enough to keep their shapes even after rinsing several times. The deposits were partially deficient or the middle of the structures were open when the line width is substantially large. Loss of the deposits at the end of each structure seen for the upper four thinner lines was probably due to the lack of dose, which was exaggerated by the subsequent nucleation and

growth processes where existing small particles facilitate the growth. These situations are very similar to those observed for the polymer deposition from the allyl-functionalized ionic liquid, where narrow lines were not likely to deposit. The specific outline structures seen for the bottom two lines may be formed by the limited supply of silver ions. Compared with the periphery of the structures that would potentially receive the ion supply from lateral directions, the middle part can only use a small number of ions originally being there. Even the barely existing ions were taken away by large grains formed at the periphery of the structures to become inside open. Of course, these speculations are made on the assumption that the nucleation and growth of the silver took longer time than the reactive species are generated by the EB: at least they should have timescales longer than that needed for scanning several tens of lines (~10 sec). These behaviors are unique to the liquid phase reactions and cannot be observed in gas or solid phase. That is, a special care should be taken when the precursor material is a part of liquid component, not the liquid itself; nevertheless the supply rate is much faster than that from the gas phase.

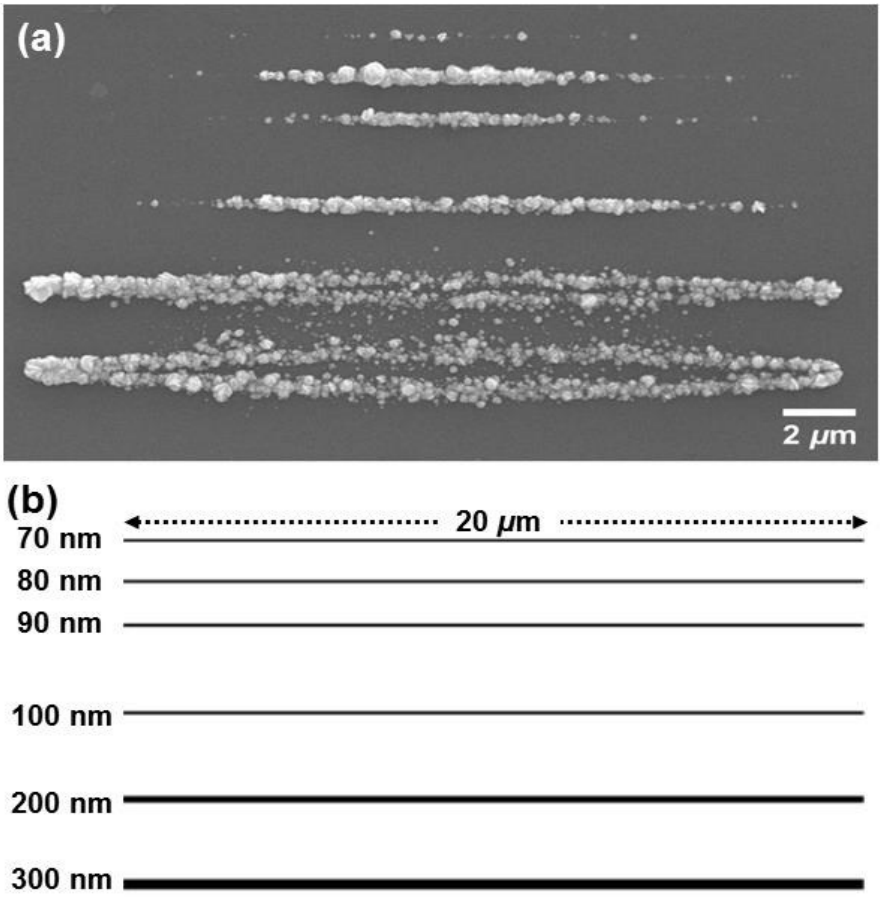

Figure 3-1. SEM image of silver structures prepared by EB irradiation to $[N_{1,1,1,3}][Tf_2N]$ containing $Ag[Tf_2N]$: (a) line structures under the dose condition of 1200 J/cm^2 and (b) the irradiation design.

Repeating EB irradiation for a long distance at a time could cause the aforementioned problems. Therefore, the same line structures designed to become perpendicular to the scanning direction to prevent the shortage of ions were made (Fig. 3-2b).

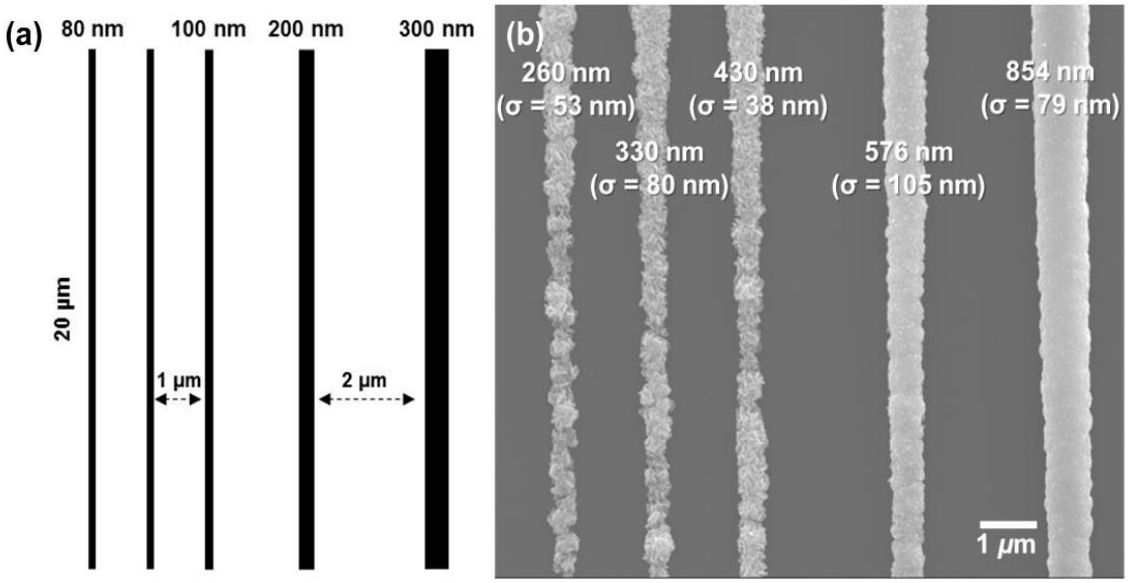

Figure 3-2. (a) The irradiation design and (b) SEM image of silver structures prepared by EB irradiation to $[N_{1,1,1,3}][Tf_2N]$ containing $Ag[Tf_2N]$. The average line widths and standard deviations for each deposited line estimated from randomly-selected ten points were given in (b).

The shapes of structures were greatly improved and no remarkable deficits were found. One unfortunate issue is that there were non-negligible differences between the widths of the drawing lines and deposited structures. The deviation is very similar to that observed for the polymer structures in chapter 2, which was attributed to the lateral spreading of electrons by scattering and diffusion of thus generated reactive species. Incidentally, when giving a lower dose (600 J/cm^2), structures except for the two thick lines on the right hand were absent (Fig. 3-3b).

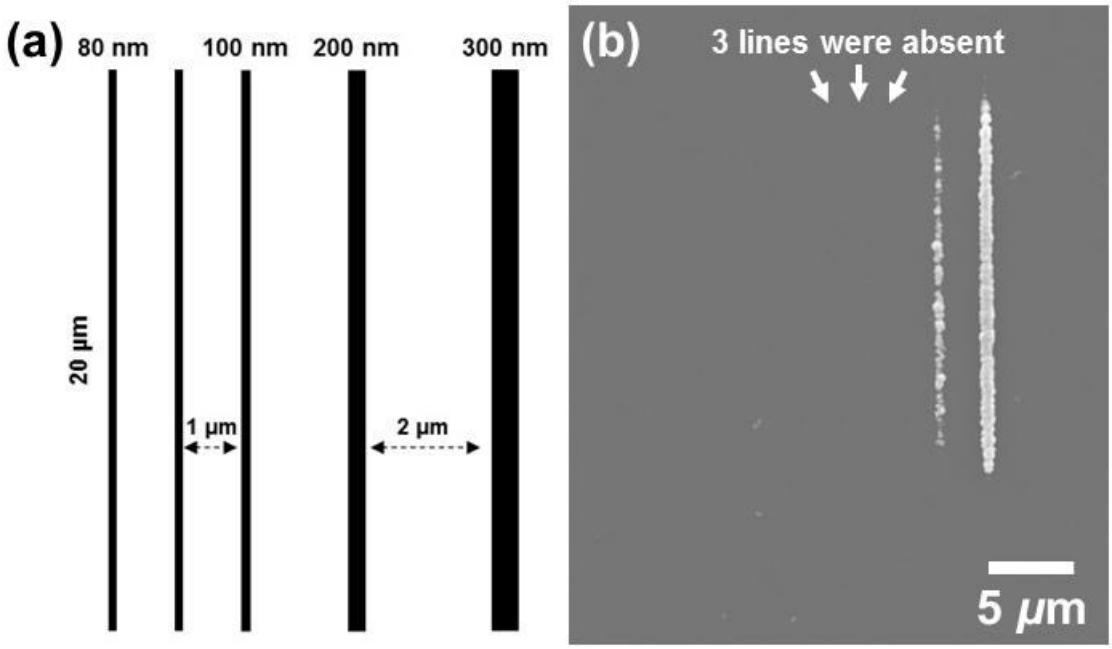

Figure 3-3. (a) The irradiation design and (b) Linear structures of silver prepared with the raster scanning of the EB perpendicular to the lines under 600 J/cm^2.

This is because they need a certain amount of dose to grow to become insoluble and being fixed on the substrate, like polymer structures needed crosslinking reaction to be solidified. By taking all of these factors into account, the Ag structures having desired shapes like Fig. 3-4a and 3-4b were obtained. The structure in Fig. 2b could be produced with the diagonal scan of EB against the readable direction.

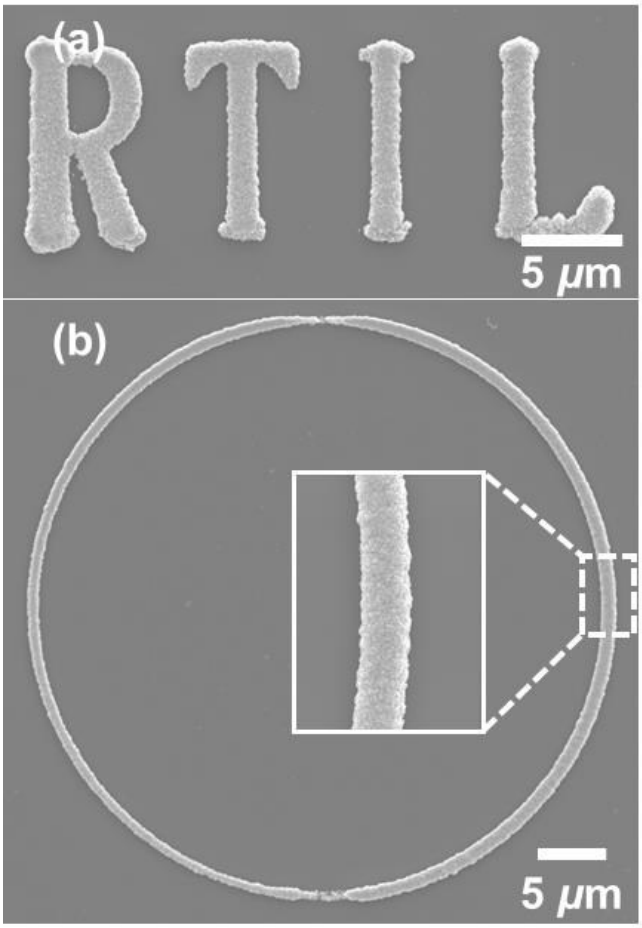

Figure 3-4. Micro-sized alphabets and (b) circular structure of 20 μm in diameter. Dose for the irradiation was set to 1200 J/cm^2.

3-3-2. Characterization of the Deposits

Another important point can be seen in the result of the Energy dispersive X-ray spectra (EDX) as shown in Fig. 3-5. The obtained deposits consisted mostly of silver with small amount of carbon as impurity (< 20 at%) that is presumably a decomposed RTIL as indicated by the Raman spectra of the deposits (see Fig. 3-6). EDX line analysis was also performed and shown in Fig. Fig. 3-7. The deposited structures consisted of silver and small amount of carbon, and no silver contamination was detected from unirradiated area. The distribution of carbon was slightly different from that of silver; it was more located at the periphery of silver and fewer existed on top of the silver, although it was detected only for the left hand of each

silver line due to the angle to the detector. Although further improvements are needed to obtain pure metals, 20 at% without a post treatment at this stage is a great progress to the fine metal structures fabricated by the EB irradiation to organometallic gas precursors. Many of them reportedly contain much amount of carbon (>50 at%) inside the structures, which cannot be fully removed even by the post treatment.[125] In comparison to them, reducing the impurities to the level that Raman signal is disappeared even on the angular silver structures was achieved by a simple post treatment dipping the substrate in a 1 M HNO_3 aqueous solution.

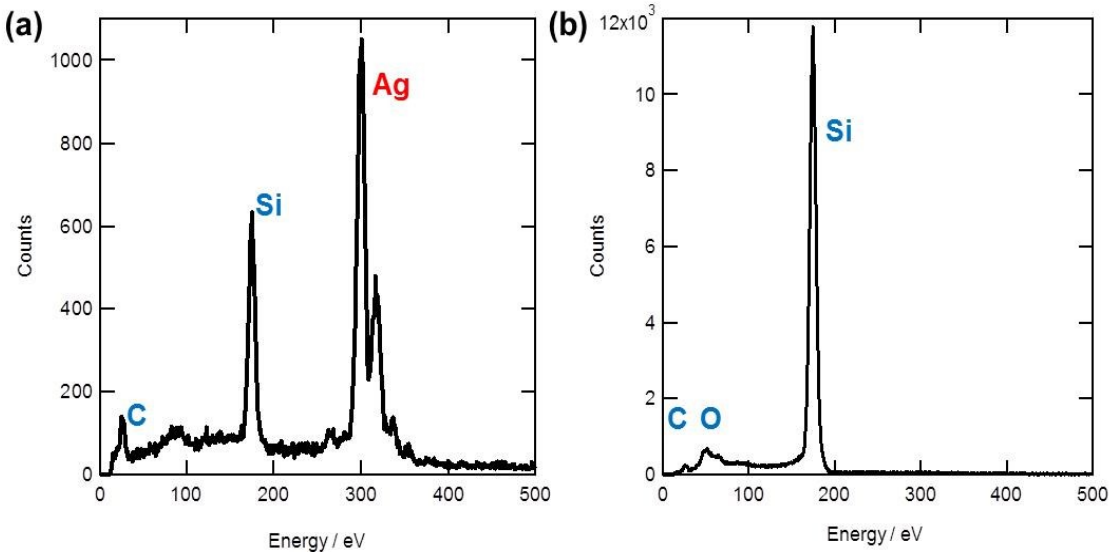

Figure 3-5. Fig. 2 EDX analyses of (a) the deposited silver patterns and (b) an EB irradiated area of the substrate. The identification for each peak was shown in the spectra.

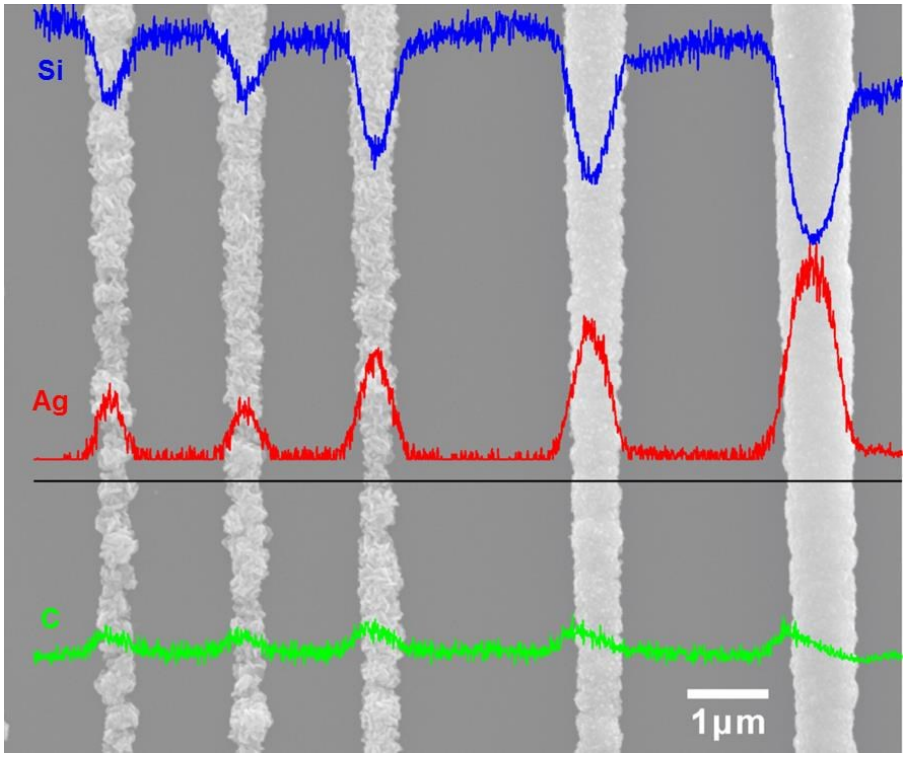

Figure 3-6. EDX line analysis of the Ag linear structures.

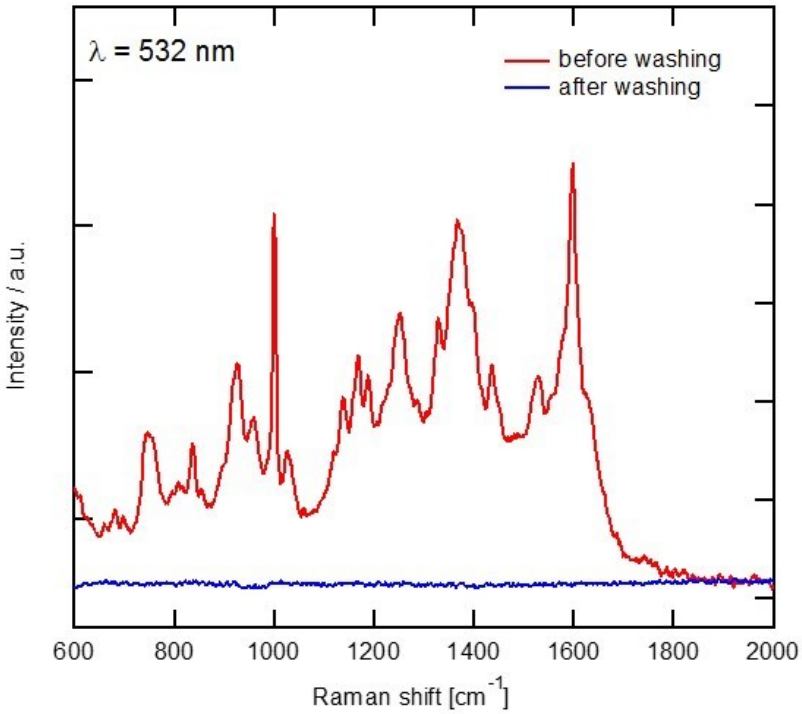

Figure 3-7. Raman spectra recorded for the Ag structures before and after the cleaning with HNO_3 solutions.

3-3-3. Discussion about the Chemical Reactions

As described above, the purity of the deposited was quite high compared to the common method. Actually, the carbon content was strongly dependent on the choice of RTIL used as a matrix. An ammonium-type RTIL, $[N_{1,1,1,3}][Tf_2N]$, which is relatively stable against the ionizing radiation according to the previous reports[41,44,126] was selected for the experiments. Still they are known to generate radiolysis products as follows:[38]

$$[R_4N][Tf_2N] \rightsquigarrow e_{solv.}^{-}, H^{+}, R_4N^{\bullet 2+}, R^{\bullet}, Tf_2N^{\bullet}, CF_3^{\bullet}, CF_3SO_2^{\bullet}$$

In fact, when imidazolium-type ionic liquids having high radiation susceptibility were used instead, the obtained structures consisted mostly of carbon (results are not shown). Alternatively, a high beam current (2.5 nA) to the $[N_{1,1,1,3}][Tf_2N]$ were applied to generate a certain amount of reactive species (radicals; R• and solvated electrons; e_{solv}^{-}) that serve as a reductant for the silver ion as follows:

$$Ag^{I} + e_{solv}^{-} \text{ or } R\bullet \rightarrow Ag^{0}$$

Ag monomers (Ag^0) thus generated would grow through some of the following equations;[127,128]

$$Ag^{0} + Ag^{I} \rightarrow Ag_2^{+}$$

$$Ag_m + Ag^{I} \rightarrow Ag_{m+1}^{+}$$

$$Ag_{m+1}^{I} + e_{solv}^{-} \rightarrow Ag_{m+1}$$

$$Ag_m + Ag^{0} \rightarrow Ag_{m+1}$$

where Ag_m corresponds to the metal nanocrystals consisting of tens to hundreds of atoms. The carbon remained in the structures may originate from the annihilation of radicals R•, like R-R. However, fortunately, they seemed to be in large part soluble to the ionic liquid so that they were washed away during the deposition of silver. These situations possibly resulted in the formation of silvers of pure, large-grain (~100 nm), and angular crystals.

3-3-4. Fabrication of the Surface-Enhanced Raman Scattering Substrate

For demonstrating the usability of thus formed silver nanostructures, SERS activity was measured. The Raman signal is known to be enhanced in a small gap between the two metal nanostructures of gold and silver.[122,129–132] Triangular silver structures was designed as inspired by the previous work, where a nano sized metal array having localized surface plasmon (LSPR) absorption in visible region was fabricated by using a template of spherical nanoparticles.[132] Figure 3-8a shows an SEM image of triangular silver structures, in which the gap between each component is controlled to be around 100 nm. As mentioned before, after several rinsing with organic solvents, very few amounts of the RTIL or carbon were remained in the silver structures and they are detected at Raman measurements. For removing them completely, the substrate was washed with 1 mM HNO_3 aqueous solutions as a pretreatment. By doing it, all peaks for them were disappeared as shown in Fig. 3-7. To measure the SERS activity of the structure, rhodamine 6G (R6G) was adsorbed on the substrate by immersing in the 10 μM aqueous solution.[129,133] Figure 3-8b shows SERS spectra of R6G obtained from the triangular silver structures. The sharp peaks at 1646, 1507, 1357 cm^{-1} derives from the C–C stretching of xanthene ring. A peak at 1571 cm^{-1} was assigned to C=O stretching, and a peak at 1181 cm^{-1} was assigned to the C–H and N–H bending vibrations of xanthene ring.[133] While detailed evidence on how much the structure contributes to the SERS intensity at this stage was not cleared enough, the effects of the size, shape, and gap of the structures on the enhancement of the Raman signal would be investigated in near future.

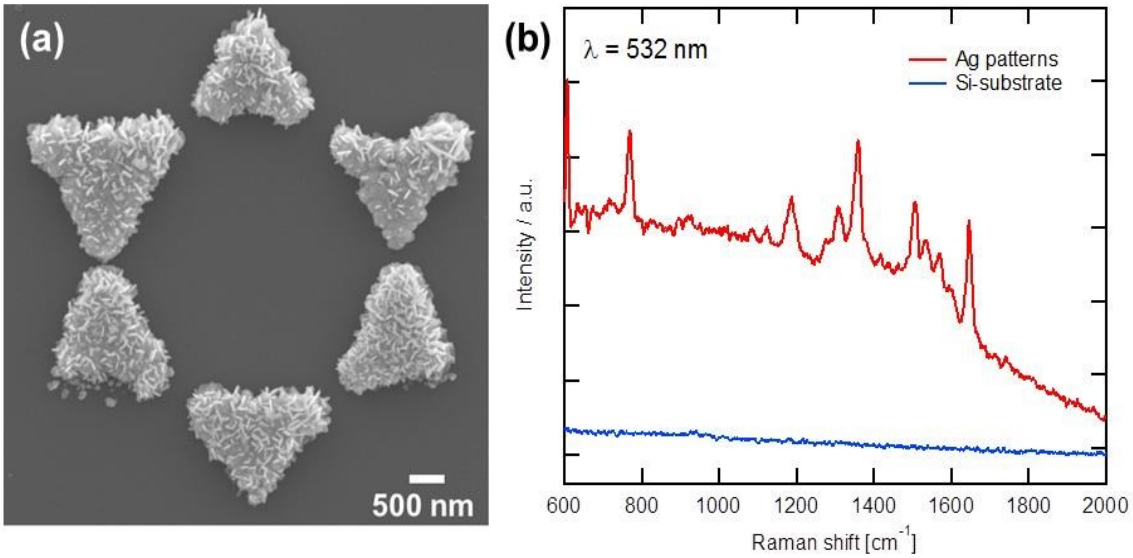

Figure 3-7. (a) SEM image of the star structure for SERS. The 23 star structures were deposited on the area of 50 μm square regularly. (b) SERS spectrum of R6G adsorbed on the structures. The red line and blue line were an Ag structure and a Si surface, respectively.

3-4. Conclusions

The new fabrication method of silver nanostructures by using the RTILs thinly coated on the Si substrate was established. The methods produced fine silver structures with high resolution around 200 nm, which is close to other direct writing techniques using the deposition from the gas phase. Although the resolution itself still has room to be improved, the purity of the silver was much higher than those previous reports because of the high solubility of the radiochemical byproducts into the ionic liquids. The silver nanostructures were found to possess SERS activity. In terms of Raman enhancement, the present method is much more advantageous compared to template methods because it is easy to fabricate arbitrary shapes at desired positions.

Summary

In this dissertation, preparation methods to fabricate various 3D polymer or metal structures have been investigated. The effect of quantum beam, such as electron beam and ion beam, to the deposited structures was also discussed. The main results and conclusions obtained in this study are summarized as follows:

In chapter 1, fabrication of three-dimensional (3D) micro/nano-polymer structures by FIB with the conventional raster scanning mode was demonstrated. It can be realized by a simple innovative approach that is an introduction of a non-volatile polymerizable room-temperature ionic liquid (RTIL) to a focused ion beam (FIB) technique that requires ultrahigh-vacuum condition. That is, various 3D micro/nano-polymer structures, even intricately-designed ones, which have never been possible to prepare by the conventional FIB method with a raster scanning mode, but can now be readily produced by this approach. Systematic fabrication of several intricate figures has revealed that the 3D structures are constructed by the manner adopted in the 3D printer. It means that just putting the polymerizable RTIL in a FIB enables the cutting-edge 3D printing technology to be built in the FIB instrument.

In chapter 2, the novel technique for fabricating three-dimensional (3D) micro/nano-polymer structures was proposed by patterning irradiation of electron beam (EB). The combination of a non-volatile polymerizable room-temperature ionic liquid (RTIL) and an EB technique enable to fabricate fine structures in liquids. By this approach, the preparation of various 3D micro/nano-polymer structures with a high resolution of sub-100 nm were achived. Further than this, the deposited structures had a high aspect ratio around 5 without any difficulties. Systematic fabrication of several structures and a theoretical calculation have revealed the 3D

structure formation mechanism. By this, the difference between the present EB and FIB method was revealed and the availability for each microfabrication method was also proposed.

In chapter 3, a novel technique for the fabrication of fine silver structures by conducting the patterning irradiation of an electron beam (EB) onto room temperature ionic liquid containing a silver salt was proposed. A simple but innovative approach that uses a RTIL enables the liquid phase reaction in an EB apparatus because of its nonvolatile property. The reduction of silver ions occurs according to the irradiating pattern to produce micro and nano silver patterns at high resolution down to around two hundreds nanometers. By doing several approaches, the important perceptions for obtaining fine structures were revealed as described in the chapter. Besides, the resulting structures contained much less amount of carbon impurities compared with those obtained from gas precursors, which is advantageous for photonic applications.

List of Publications

1. Three-dimensional micro/nano-scale structure fabricated by combination of non-volatile polymerizable RTIL and FIB irradiation

   Susumu Kuwabata, Hiro Minamimoto, Kosuke Ionue, Akihito Imanishi, Ken Hosoya, Hiroshi Uyama, Tsukasa Torimoto, Tetsuya Tsuda, and Shu Seki

   Scientific Reports, 2014, 4, 3722.

2. Polymerization of Room-Temperature Ionic Liquid Monomers by Electron Beam Irradiation with the Aim of Fabricating Three- Dimensional Micropolymer/ Nanopolymer Structures

   Hiro Minamimoto, Haruyasu Irie, Taro Uematsu, Tetsuya Tsuda, Akihito Imanishi, Shu Seki, and Susumu Kuwabata

   Langmuir, 2014, Electronic published as ASAP. This paper was selected as the *Editor's choice.*

3. Fine Patterning of Silver Metal by Electron Beam Irradiation onto Room- Temperature Ionic Liquid

   Hiro Minamimoto, Haruyasu Irie, Taro Uematsu, Tetsuya Tsuda, Akihito Imanishi, Shu Seki, and Susumu Kuwabata

   Chemistry Letters, 2015, in press. This paper was selected as the *Editor's choice.*

References

[1] K. K. B. Hon, L. Li, I. M. Hutchings, *CIRP Ann. - Manuf. Technol.* **2008**, *57*, 601–620.

[2] V. J. Cadarso, K. Pfeiffer, U. Ostrzinski, J. B. Bureau, G. a Racine, A. Voigt, G. Gruetzner, J. Brugger, *J. Micromechanics Microengineering* **2011**, *21*, 017003.

[3] H. Wang, G. Zheng, W. Li, X. Wang, D. Sun, *Appl. Phys. A* **2011**, *102*, 457–461.

[4] P. Kunwar, J. Hassinen, G. Bautista, R. H. A. Ras, J. Toivonen, *ACS Nano* **2014**, *8*, 11165–71.

[5] J. A van Kan, A. A Bettiol, F. Watt, *Nano Lett.* **2006**, *6*, 579–82.

[6] F. Watt, *Nucl. Instruments Methods Phys. Res. Sect. B* **1999**, *158*, 165–172.

[7] E. Zanchetta, G. Della Giustina, G. Grenci, A. Pozzato, M. Tormen, G. Brusatin, *Adv. Mater.* **2013**, *25*, 6261–5.

[8] Y. Xia, G. M. Whitesides, *Annu. Rev. Mater. Sci.* **1998**, *28*, 153–184.

[9] A. N. Broers, A. C. F. Hoole, J. M. Ryan, *Microelectron. Eng.* **1996**, *32*, 131–142.

[10] C. Vieu, F. Carcenac, A. Pépin, Y. Chen, M. Mejias, A. Lebib, L. Manin-Ferlazzo, L. Couraud, H. Launois, *Appl. Surf. Sci.* **2000**, *164*, 111–117.

[11] H. Lorenz, M. Despont, N. Fahrni, N. LaBianca, P. Renaud, P. Vettiger, *J. Micromech. Microeng.* **1997**, *7*, 121–124.

[12] D. R. S. Cumming, S. Thoms, S. P. Beaumont, J. M. R. Weaver, *Appl. Phys. Lett.* **1996**, *68*, 322.

[13] T. H. P. Chang, M. Mankos, K. Y. Lee, L. P. Muray, *Microelectron. Eng.* **2001**, *57-58*, 117–135.

[14] K. Y. Lee, *J. Vac. Sci. Technol. B Microelectron. Nanom. Struct.* **1993**, *11*, 2807.

[15] I. Utke, P. Hoffmann, J. Melngailis, *J. Vac. Sci. Technol. B Microelectron. Nanom. Struct.* **2008**, *26*, 1197.

[16] K. Mølhave, D. N. Madsen, A. M. Rasmussen, A. Carlsson, C. C. Appel, M. Brorson, C. J. H. Jacobsen, P. Bøggild, *Nano Lett.* **2003**, *3*, 1499–1503.

[17] P. D. Rack, J. D. Fowlkes, S. J. Randolph, *Nanotechnology* **2007**, *18*, 465602.

[18] H. Plank, C. Gspan, M. Dienstleder, G. Kothleitner, F. Hofer, *Nanotechnology* **2008**, *19*, 485302.

[19] I. Utke, P. Hoffmann, B. Dwir, K. Leifer, E. Kapon, P. Doppelt, *J. Vac. Sci. Technol. B* **2000**, *18*, 3168.

[20] I. A. Shkrob, T. W. Marin, S. D. Chemerisov, J. Hatcher, J. F. Wishart, *J. Phys. Chem. B* **2012**, *116*, 9043–55.

[21] C. C. Chu, N. D. Campbell, *J. Biomed. Mater. Res.* **1982**, *16*, 417–30.

[22] W. Huang, Y. Fu, C. Wang, Y. Xu, Y. Chen, *J. Appl. Polym. Sci.* **2003**, *89*, 3437–3441.

[23] A. Henglein, *J. Phys. Chem.* **1959**, *63*, 1852–1858.

[24] Y. Maeyoshi, K. Takano, A. Asano, H. Marui, M. Omichi, T. Satoh, T. Kamiya, Y. Ishii, T. Ohkubo, M. Koka, et al., *Jpn. J. Appl. Phys.* **2012**, *51*, 045201.

[25] I. A. Shkrob, T. W. Marin, S. D. Chemerisov, J. F. Wishart, *J. Phys. Chem. B* **2011**, *115*, 3872–88.

[26] I. A. Shkrob, T. W. Marin, S. D. Chemerisov, J. L. Hatcher, J. F. Wishart, *J. Phys. Chem. B* **2011**, *115*, 3889–902.

[27] A. Marcinek, J. Zielonka, J. Gębicki, C. M. Gordon, I. R. Dunkin, *J. Phys. Chem. A* **2001**, *105*, 9305–9309.

[28] Y. Katsumura, S. Tagawa, Y. Tabata, *J. Phys. Chem.* **1980**, *84*, 833–839.

[29] H. Shiraishi, Y. Katsumura, D. Hiroishi, K. Ishigure, M. Washio, *J. Phys. Chem.* **1988**, *92*, 3011–3017.

[30] M. Simic, P. Neta, E. Hayon, *J. Phys. Chem.* **1969**, *73*, 3794–3800.

[31] M. Bietti, E. Baciocchi, S. Steenken, *J. Phys. Chem. A* **1998**, *102*, 7337–7342.

[32] R. D. Rogers, K. R. Seddon, *Science* **2003**, *302*, 792–3.

[33] F. Endres, M. Bukowski, R. Hempelmann, H. Natter, *Angew. Chem. Int. Ed. Engl.* **2003**, *42*, 3428–30.

[34] M. J. Earle, J. M. S. S. Esperança, M. a Gilea, J. N. C. Lopes, L. P. N. Rebelo, J. W. Magee, K. R. Seddon, J. a Widegren, *Nature* **2006**, *439*, 831–4.

[35] M. Armand, F. Endres, D. R. MacFarlane, H. Ohno, B. Scrosati, *Nat. Mater.* **2009**, *8*, 621–9.

[36] J. Y. Huang, L. Zhong, C. M. Wang, J. P. Sullivan, W. Xu, L. Q. Zhang, S. X. Mao, N. S. Hudak, X. H. Liu, A. Subramanian, et al., *Science* **2010**, *330*, 1515–20.

[37] J. F. Wishart, P. Neta, *J. Phys. Chem. B* **2003**, *107*, 7261–7267.

[38] J. Grodkowski, P. Neta, *J. Phys. Chem. A* **2002**, *106*, 5468–5473.

[39] I. A. Shkrob, S. D. Chemerisov, J. F. Wishart, *J. Phys. Chem. B* **2007**, *111*, 11786–93.

[40] K. Takahashi, T. Sato, Y. Katsumura, J. Yang, T. Kondoh, Y. Yoshida, R. Katoh, *Radiat. Phys. Chem.* **2008**, *77*, 1239–1243.

[41] I. A. Shkrob, J. F. Wishart, *J. Phys. Chem. B* **2009**, *113*, 5582–92.

[42] J. F. Wishart, S. I. Lall-Ramnarine, R. Raju, A. Scumpia, S. Bellevue, R. Ragbir, R. Engel, *Radiat. Phys. Chem.* **2005**, *72*, 99–104.

[43] D. Allen, G. Baston, A. E. Bradley, T. Gorman, A. Haile, I. Hamblett, J. E. Hatter, M. J. F. Healey, B. Hodgson, R. Lewin, et al., *Green Chem.* **2002**, *4*, 152–158.

[44] T. Tsuda, T. Sakamoto, Y. Nishimura, S. Seino, A. Imanishi, S. Kuwabata, *Chem. Commun.*. **2012**, *48*, 1925–7.

[45] P. Roy, R. Lynch, P. Schmuki, *Electrochem. commun.* **2009**, *11*, 1567–1570.

[46] M. Galiński, A. Lewandowski, I. Stępniak, *Electrochim. Acta* **2006**, *51*, 5567–5580.

[47] V. I. Pârvulescu, C. Hardacre, *Chem. Rev.* **2007**, *107*, 2615–65.

[48] N. V Plechkova, K. R. Seddon, *Chem. Soc. Rev.* **2008**, *37*, 123–50.

[49] E. F. Smith, I. J. V. Garcia, D. Briggs, P. Licence, *Chem. Commun.* **2005**, 5633–5.

[50] S. Kuwabata, A. Kongkanand, D. Oyamatsu, T. Torimoto, *Chem. Lett.* **2006**, *35*, 600–601.

[51] S. Arimoto, M. Sugimura, H. Kageyama, T. Torimoto, S. Kuwabata, *Electrochim. Acta* **2008**, *53*, 6228–6234.

[52] T. Tsuda, N. Nemoto, K. Kawakami, E. Mochizuki, S. Kishida, T. Tajiri, T. Kushibiki, S. Kuwabata, *Chembiochem* **2011**, *12*, 2547–50.

[53] S. Arimoto, D. Oyamatsu, T. Torimoto, S. Kuwabata, *Chemphyschem* **2008**, *9*, 763–7.

[54] A. Imanishi, M. Tamura, S. Kuwabata, *Chem. Commun.* **2009**, 1775–7.

[55] A. Imanishi, S. Gonsui, T. Tsuda, S. Kuwabata, K. Fukui, *Phys. Chem. Chem. Phys.* **2011**, *13*, 14823–30.

[56] T. Uematsu, M. Baba, Y. Oshima, T. Tsuda, T. Torimoto, S. Kuwabata, *J. Am. Chem. Soc.* **2014**, *136*, 13789–97.

[57] A. Delcorte, B. J. Garrison, R. Samson, **2006**, *252*, 6419–6422.

[58] D. Kern, T. Kuech, M. Oprysko *et al.*, *Science.* **1988**, *241*, 963-944.

[59] K. Gamo, *Semicond. Sci. Technol.* **1993**, *8*, 1118–1123.

[60] H. H. Chen, O. a Urquidez, S. Ichim, L. H. Rodriquez, M. P. Brenner, M. J. Aziz, *Science* **2005**, *310*, 294–7.

[61] J. Valentine, S. Zhang, T. Zentgraf, E. Ulin-Avila, D. a Genov, G. Bartal, X. Zhang, *Nature* **2008**, *455*, 376–9.

[62] J. Han, H. Lee, B.-K. Min, S. J. Lee, *Microelectron. Eng.* **2010**, *87*, 1–9.

[63] S. Matsui, T. Kaito, J. Fujita, M. Komuro, K. Kanda, Y. Haruyama, *J. Vac. Sci. Technol. B* **2000**, *18*, 3181.

[64] T. Hoshino, K. Watanabe, R. Kometani, T. Morita, K. Kanda, Y. Haruyama, T. Kaito, J. Fujita, M. Ishida, Y. Ochiai, et al., *J. Vac. Sci. Technol. B* **2003**, *21*, 2732.

[65] S. Matsui, *Nucl. Instruments Methods Phys. Res. Sect. B* **2007**, *257*, 758–764.

[66] S. Amajjahe, H. Ritter, *Macromolecules* **2008**, *41*, 716–718.

[67] M. D. Green, D. Salas-de la Cruz, Y. Ye, J. M. Layman, Y. a. Elabd, K. I. Winey, T. E. Long, *Macromol. Chem. Phys.* **2011**, *212*, 2522–2528.

[68] D. F. S. Petri, G. Wenz, P. Schunk, T. Schimmel, *Langmuir* **1999**, 15, 4520–4523.

[69] E. R. Talaty, S. Raja, V. J. Storhaug, A. Dölle, W. R. Carper, *J. Phys. Chem. B* **2004**, *108*, 13177–13184.

[70] R. C. Laible, *Chem. Rev.* **1958**, *58*, 807–843.

[71] R. Kometani, S. Ishihara, *Sci. Technol. Adv. Mater.* **2009**, *10*, 034501.

[72] J. Igaki, K. Kanda, Y. Haruyama, M. Ishida, Y. Ochiai, J. Fujita, T. Kaito, S. Matsui, *Microelectron. Eng.* **2006**, *83*, 1225–1228.

[73] Z. Chang, J. a. LaVerne, *J. Phys. Chem. B* **2000**, *104*, 10557–10562.

[74] S. Tsukuda, S. Seki, M. Sugimoto, S. Tagawa, *Jpn. J. Appl. Phys.* **2005**, *44*, 5839–5842.

[75] G. Y. Gerasimov, *J. Eng. Phys. Thermophys.* **2011**, *84*, 947–963.

[76] S. Tagawa, S. Tsukuda, S. Seki, M. Sugimoto, T. Sato, M. Oikawa, T. Sakai, *Surf. Coatings Technol.* **2007**, *201*, 8495–8498.

[77] J. F. Ziegler, M. D. Ziegler, J. P. Biersack, *Nucl. Instruments Methods Phys. Res. Sect. B Beam Interact. with Mater. Atoms* **2010**, *268*, 1818–1823.

[78] H. Erramli, O. Elbounagui, M. a. Misdaq, a. Merzouki, *Nucl. Instruments Methods Phys. Res. Sect. B* **2007**, *263*, 127–131.

[79] T. R. Groves, D. Pickard, B. Rafferty, N. Crosland, D. Adam, G. Schubert, *Microelectron. Eng.* **2002**, *61-62*, 285–293.

[80] H. G. Craighead, *J. Appl. Phys.* **1984**, *55*, 4430.

[81] I. Zailer, J. E. F. Frost, V. Chabasseur-Molyneux, C. J. B. Ford, M. Pepper, *Semicond. Sci. Technol.* **1996**, *11*, 1235–1238.

[82] J. Fujita, Y. Ohnishi, Y. Ochiai, S. Matsui, *Appl. Phys. Lett.* **1996**, *68*, 1297.

[83] W. Walter Hu, K. Sarveswaran, M. Lieberman, G. H. Bernstein, *J. Vac. Sci. Technol. B* **2004**, *22*, 1711.

[84] P. B. Fischer, S. Y. Chou, *Appl. Phys. Lett.* **1993**, *62*, 2989.

[85] M. Hatzakis, *J. Electrochem. Soc.* **1991**, *138*, 1076.

[86] P. Argitis, *J. Vac. Sci. Technol. B Microelectron. Nanom. Struct.* **1995**, *13*, 3030.

[87] K. Natsuda, T. Kozawa, K. Okamoto, S. Tagawa, *Jpn. J. Appl. Phys.* **2007**, *46*, 7285–7289.

[88] T. Kozawa, Y. Yoshida, M. Uesaka, S. Tagawa, *Jpn. J. Appl. Phys.* **1992**, *31*, 4301–4306.

[89] U. C. Coskun, H. Mebrahtu, P. B. Huang, J. Huang, D. Sebba, A. Biasco, A. Makarovski, A. Lazarides, T. H. LaBean, G. Finkelstein, *Appl. Phys. Lett.* **2008**, *93*, 123101.

[90] J. Domke, M. Radmacher, *Langmuir* **1998**, *14*, 3320–3325.

[91] M. J. Bojdys, J.-O. Müller, M. Antonietti, A. Thomas, *Chemistry* **2008**, *14*, 8177–82.

[92] L. Berthon, S. I. Nikitenko, I. Bisel, C. Berthon, M. Faucon, B. Saucerotte, N. Zorz, P. Moisy, *Dalton Trans.* **2006**, 2526–34.

[93] C. Reynaud, F. Sommer, C. Quet, N. El Bounia, T. M. Duc, *Surf. Interface Anal.* **2000**, *30*, 185–189.

[94] A. Noda, K. Hayamizu, M. Watanabe, *J. Phys. Chem. B* **2001**, *105*, 4603–4610.

[95] H. Fu, Z. Xing, X. Cao, G. Wu, *Chinese Sci. Bull.* **2012**, *57*, 2752–2758.

[96] D. Drouin, A. R. Couture, D. Joly, X. Tastet, V. Aimez, R. Gauvin, *Scanning* **2007**, *29*, 92–101.

[97] F. J. Pantenburg, *J. Vac. Sci. Technol. B Microelectron. Nanom. Struct.* **1998**, *16*, 3547.

[98] B. Radha, S. Kiruthika, G. U. Kulkarni, *J. Am. Chem. Soc.* **2011**, *133*, 12706–13.

[99] T. Bhuvana, G. U. Kulkarni, *ACS Nano* **2008**, *2*, 457–62.

[100] H. Lee, S. Hong, K. Yang, K. Choi, *Appl. Phys. Lett.* **2006**, *88*, 143112.

[101] V. Halka, M. J. Schmid, V. Avrutskiy, X. Ma, R. Schuster, *Angew. Chem. Int. Ed. Engl.* **2011**, *50*, 4692–5.

[102] P. Hoffmann, G. Ben Assayag, J. Gierak, J. Flicstein, M. Maar-Stumm, H. van den Bergh, *J. Appl. Phys.* **1993**, *74*, 7588.

[103] M. K. Corbierre, J. Beerens, R. B. Lennox, *Chem. Mater.* **2005**, *17*, 5774–5779.

[104] P. Schmuki, L. E. Erickson, *Phys. Rev. Lett.* **2000**, *85*, 2985–8.

[105] E. Delamarche, J. Vichiconti, S. a. Hall, M. Geissler, W. Graham, B. Michel, R. Nunes, *Langmuir* **2003**, *19*, 6567–6569.

[106] J. M. Steigerwald, S. P. Murarka, R. J. Gutmann, D. J. Duquette, *Mater. Chem. Phys.* **1995**, *41*, 217–228.

[107] P. Calvert, *Chem. Mater.* **2001**, *13*, 3299–3305.

[108] M. Singh, H. M. Haverinen, P. Dhagat, G. E. Jabbour, *Adv. Mater.* **2010**, *22*, 673–85.

[109] W. S. Wong, E. M. Chow, R. Lujan, V. Geluz-Aguilar, M. L. Chabinyc, *Appl. Phys. Lett.* **2006**, *89*, 142118.

[110] S. B. Fuller, E. J. Wilhelm, J. M. Jacobson, *J. Microelectromechanical Syst.* **2002**, *11*, 54–60.

[111] W.-E. Lu, Y.-L. Zhang, M.-L. Zheng, Y.-P. Jia, J. Liu, X.-Z. Dong, Z.-S. Zhao, C.-B. Li, Y. Xia, T.-C. Ye, et al., *Opt. Mater. Express* **2013**, *3*, 1660.

[112] K. Kordás, K. Bali, S. Leppävuori, A. Uusimäki, L. Nánai, *Appl. Surf. Sci.* **1999**, *152*, 149–155.

[113] T. Baldacchini, A.-C. Pons, J. Pons, C. N. LaFratta, J. T. Fourkas, Y. Sun, M. J. Naughton, *Opt. Express* **2005**, *13*, 1275.

[114] K. Kordás, J. Békési, R. Vajtai, L. Nánai, S. Leppävuori, A. Uusimäki, K. Bali, T. F. George, G. Galbács, F. Ignácz, et al., *Appl. Surf. Sci.* **2001**, *172*, 178–189.

[115] A. Luisier, I. Utke, T. Bret, F. Cicoira, R. Hauert, S.-W. Rhee, P. Doppelt, P. Hoffmann, *J. Electrochem. Soc.* **2004**, *151*, C590.

[116] M. Shimojo, S. Bysakh, K. Mitsuishi, M. Tanaka, M. Song, K. Furuya, *Appl. Surf. Sci.* **2005**, *241*, 56–60.

[117] G. C. Gazzadi, S. Frabboni, C. Menozzi, *Nanotechnology* **2007**, *18*, 445709.

[118] Y. Kakefuda, Y. Yamashita, K. Mukai, J. Yoshinobu, *Surf. Sci.* **2007**, *601*, 5108–5111.

[119] Y. R. Choi, P. D. Rack, B. Frost, D. C. Joy, *Scanning* **2007**, *29*, 171–6.

[120] T. Tsuda, T. Sakamoto, Y. Nishimura, S. Seino, A. Imanishi, K. Matsumoto, R. Hagiwara, T. Uematsu, S. Kuwabata, *RSC Adv.* **2012**, *2*, 11801.

[121] V. K. Sharma, R. a Yngard, Y. Lin, *Adv. Colloid Interface Sci.* **2009**, *145*, 83–96.

[122] M. G. Albrecht, J. A. Creighton, *J. Am. Chem. Soc.* **1977**, *99*, 5215–5217.

[123] F. Agel, F. Pitsch, F. F. Krull, P. Schulz, M. Wessling, T. Melin, P. Wasserscheid, *Phys. Chem. Chem. Phys.* **2011**, *13*, 725–31.

[124] S.-J. Huo, X.-K. Xue, Q.-X. Li, S.-F. Xu, W.-B. Cai, *J. Phys. Chem. B* **2006**, *110*, 25721–8.

[125] A. Botman, J. J. L. Mulders, C. W. Hagen, *Nanotechnology* **2009**, *20*, 372001.

[126] J. F. Wishart, *J. Phys. Chem. Lett.* **2010**, *1*, 3225–3231.

[127] J. Belloni, *Catal. Today* **2006**, *113*, 141–156.

[128] B. Soroushian, I. Lampre, J. Belloni, M. Mostafavi, *Radiat. Phys. Chem.* **2005**, *72*, 111–118.

[129] L. Gunnarsson, E. J. Bjerneld, H. Xu, S. Petronis, B. Kasemo, M. Käll, *Appl. Phys. Lett.* **2001**, *78*, 802.

[130] T. Konishi, M. Kiguchi, M. Takase, F. Nagasawa, H. Nabika, K. Ikeda, K. Uosaki, K. Ueno, H. Misawa, K. Murakoshi, *J. Am. Chem. Soc.* **2013**, *135*, 1009–14.

[131] C. L. Haynes, R. P. Van Duyne, *J. Phys. Chem. B* **2001**, *105*, 5599–5611.

[132] K. A Willets, R. P. Van Duyne, *Annu. Rev. Phys. Chem.* **2007**, *58*, 267–97.

[133] M. L. Coluccio, G. Das, F. Mecarini, F. Gentile, A. Pujia, L. Bava, R. Tallerico, P. Candeloro, C. Liberale, F. De Angelis, et al., *Microelectron. Eng.* **2009**, *86*, 1085–1088.

Acknowledgements

First of all, the author would like to express his great gratitude to Prof. Susumu Kuwabata, Department of Applied Chemistry, Graduate School of Engineering, Osaka University, for his continuous guidance, invaluable suggestions, and encouragement throughout the course of thesis.

The author would also like to thank to Prof. Nobuhito Imanaka, and Prof. Takahiro Kozawa, Department of Applied Chemistry, Graduate School of Engineering, Osaka University, for their helpful advices.

The author would like to express his special thanks to Associate Prof. Tetsuya Tsuda, Assistant Prof. Taro Uematsu, Department of Applied Chemistry, Graduate School of Engineering, Osaka University, for their helpful suggestion and valuable discussion. Their critical and appropriate advices always led the author to much success in this research.

The author deeply thank Dr. Eiko Mochizuki, Department of Applied Chemistry, Graduate School of Engineering, Osaka University, for her hearty encouragement and grateful help throughout the life in the laboratory.

The author would like to express his thanks to Associate Prof. Akihito Imanishi, Department of Chemistry, Graduate School of Engineering Science, Osaka University, and Prof. Shu Seki, Department of Applied Chemistry, Graduate School of Engineering, Osaka University, for their expert comment and experimental help.

The author has greatly benefited from Prof. James F. Wishart, Chemistry Department, Brookhaven National Laboratory, USA, for his help and giving the author precious experiences.

The author is grateful acknowledge to Mr. Haruyasu Irie and Dr. Kazuki Yoshii for their experimental support and discussion. The author is also grateful to Mr. Shigeo Maeda, Dr. Yi-Ting Hsieh, Mrs. Shoko Kishida, Mrs. Reiko Izumi, Mr. Hiroshi Tenmyo, Mr. Koshi

Kawakami, Mr. Koshiro Kondo, Mr. Taiki Sakamoto, Mr. Yuichi Ikeda, Mr. Akihisa Doko, Mr. Yoshitomo Nishimura, Mr. Jun-Tae Han, Mr. Yusuke Kaji, Mr. Masakatsu Kawabata, Mr. Tsukasa Kanetsuku, Mr. Masahiro Baba, Mr. Yuki Iwasaki, Mr. Masami Sasatani, Mr. Haruki Narikawa, Mr. Taisuke Asano, Mr. Kazuki Iwasaki, Mr. Itsuki Kokubo, Mr. Tsuyoshi Sakamoto, Mr. Keisuke Yamaji, Mr. Sayaki Umemoto, Mr. Atsushi Ohta, Mr. Teruki Sano, Mr. Eisuke Shimomura, Mr. Amane Sawamura, Mr. Kiryu Sato, Mr. Yu Hashimoto, Mr. Go Matsui and all other members in Applied Electrochemistry Laboratory for hearty support and unforgettable memories.

Finally, the author wishes to express his deeply gratitude to his parents, Osao Minamimoto and Terumi Minamimoto, his sister, Miwa Okawa, his brother, Tetsuo Minamimoto, and his grandparents, the late Teruo Sawa, Umeko Sawa and the late Fumiko Minamimoto for their hearty encouragement and support. Without them, the author could never have achieved this research.

January, 2015

Hiro Minamimoto